

REPORT DOCUMENTATION PAGE

AFRL-SR-AR-TR-04-

The public reporting burden for this collection of information is estimated to average 1 hour per response, including the gathering and maintaining the data needed, and completing and reviewing the collection of information. Send comments regarding this burden estimate or any other aspect of this collection of information, including suggestions for reducing the burden, to Department of Defense, Washington Headquarters Services, Directorate for Information Operations and Reports, 1215 Jefferson Davis Highway, Suite 1204, Arlington, VA 22202-4302. Respondents should be aware that notwithstanding any other notation that may appear hereon, no person shall be subject to any penalty for failing to comply with a collection of information if it does not display a currently valid OMB control number.

PLEASE DO NOT RETURN YOUR FORM TO THE ABOVE ADDRESS.

0426

1. REPORT DATE (DD-MM-YYYY) 05/07/2004		2. REPORT TYPE FINAL		3. DATES COVERED (From - To) December 1, 2000 - April 30, 2004	
4. TITLE AND SUBTITLE Investigation of Electromagnetic Field Propagation in Reverse Saturable Absorbers				5a. CONTRACT NUMBER	
				5b. GRANT NUMBER AFOSR F49620-01-1-0086	
				5c. PROGRAM ELEMENT NUMBER	
				5d. PROJECT NUMBER	
6. AUTHOR(S) McLaughlin, David W. Potasek, Mary				5e. TASK NUMBER	
				5f. WORK UNIT NUMBER	
7. PERFORMING ORGANIZATION NAME(S) AND ADDRESS(ES) Courant Institute of Mathematical Sciences - New York University 251 Mercer Street New York, NY 10012				8. PERFORMING ORGANIZATION REPORT NUMBER	
9. SPONSORING/MONITORING AGENCY NAME(S) AND ADDRESS(ES) Air Force Office of Scientific Research / NM 4015 Wilson Boulevard Arlington, VA 22203				10. SPONSOR/MONITOR'S ACRONYM(S)	
				11. SPONSOR/MONITOR'S REPORT NUMBER(S)	
12. DISTRIBUTION/AVAILABILITY STATEMENT Distribution Unlimited					
13. SUPPLEMENTARY NOTES					
14. ABSTRACT We have developed and implemented a numerical technique for the propagation of the electromagnetic field in a five-level reverse saturable absorber medium, which includes the nonlinear Kerr effect and dispersion. The numerical method combines a split step beam propagation method with the Crank-Nicholson method. Our numerical results and calculations enable the prediction of nonlinear absorption using experimentally measurable material parameters such as the absorption cross-sections and decay rates. We also investigated the interplay between the optical pulse properties such as the temporal pulse width, spatial radius, incident energy and the carrier dynamics, and nonlinear absorption of the reverse saturable absorber.					
15. SUBJECT TERMS optical limiters, lasers, nonlinear optics, electromagnetics					
16. SECURITY CLASSIFICATION OF:			17. LIMITATION OF ABSTRACT none	18. NUMBER OF PAGES 50	19a. NAME OF RESPONSIBLE PERSON Dr. David W. McLaughlin / Dr. Mary Potasek
a. REPORT U	b. ABSTRACT U	c. THIS PAGE U			19b. TELEPHONE NUMBER (Include area code) (212) 998-2415 / (212) 998-3144

20040830 048

Standard Form 298 (Rev. 8/98)
Prescribed by ANSI Std. Z39.18

BEST AVAILABLE COPY

Contents

1. Introduction.....	1
2. Mechanisms of Optical Limiting.....	3
2.1 Kerr Nonlinear Refraction.....	3
2.2 Nonlinear Scattering.....	4
2.3 Two Photon Absorption.....	4
2.4 Semiconductor Nonlinearity.....	5
2.5 Thermal Nonlinearity.....	5
2.6 Reverse Saturable Absorption.....	6
3. RSA Materials.....	6
3.1 Fullerenes-Carbon 60 / Carbon 70.....	7
3.2 Porphyrin And Related Derivatives.....	7
4. General five level model for RSA.....	8
4.1 Rate Equations.....	8
4.2 Intensity Equations.....	8
5. Numerical Method.....	11
5.1 Numerical Method and Operator Equations.....	12
5.2 Propagation Equation.....	14
6. Results And Discussion.....	15
6.1 Initial Results.....	15
6.2 Three Distinctive Regions.....	16
6.3 Propagation Through RSA Material in Kerr Medium.....	17
6.4 Pulse Shaping Techniques.....	17
6.5 Spatial Pulse Shaping: Self-focusing.....	17
6.6 Temporal Pulse Shaping Techniques.....	18
6.7 Self-focusing and RSA.....	18
6.8 Multiple Pulses.....	18
7. Conclusions.....	19
Bibliography.....	21
Appendix.....	27

Investigation of Electromagnetic Field Propagation in Reverse Saturable Absorbers

1. Introduction

The general area of nonlinear absorbers/optical limiting has grown substantially over the last two decades. There is increasing interest in various mechanisms of optical limiting. A number of review articles and conference reports demonstrate the vitality of this subject [1]-[11]. In general, an optical limiter keeps the power, intensity, energy or energy density transmitted by an optical system below a predetermined maximum value that is independent of the size of the input pulse while maintaining a high transmittance at low input power. The many applications of the device include laser power regulation, laser mode-locking, optical pulse shaping, signal level processing, and sensor/detector protection.

Importantly, the device must operate within a fast enough response time to protect a sensor or regulate pulsed laser sources. The transmission must be reduced in a time period shorter than the pulse width. With laser pulse durations ranging from milliseconds to femtoseconds, electrooptic devices such as electrooptic switches that operate on the nanosecond time scale are often too slow. On the other hand, passive devices use a nonlinear optical medium that has a fast response time and acts as a sensor, processor and modulator [8]. However, typical nonlinear materials are not sufficient optical limiters by themselves. As a result, the passive system places the nonlinear optical components in or near a focal plane. The focal point should be located near the exit plane of the material to utilize the entire path length.

The laser threat occurs at wavelengths within the transparency window of the atmosphere. Thus the most dangerous laser sources will be in the following windows: visible-near infrared region between $0.4\mu\text{m}$ and $1.4\mu\text{m}$; infrared region I (IR I) window between $1.5\mu\text{m}$ and $2.7\mu\text{m}$, infrared region II (IR II) window between $3\mu\text{m}$ and $5.8\mu\text{m}$ and infrared region III (IR III) window between $7.5\mu\text{m}$ and $14\mu\text{m}$. The optical limiters working inside these wavelength ranges are of unparalleled importance. The main types of detectors fall into two categories; namely, direct (eye) and indirect (photo detector, image intensifiers and IR night vision sensors).

The maximum permissible transmitted energy is dependent on many factors including the optical wavelength, pulse width, linear transmittance, maximum output, f/number of the system, damage threshold and stability. The various situations not only cover a very wide range of wavelengths, which includes infrared and the whole visual range but also require different types of optical limiter mechanisms, e.g. fluence limiter, energy limiter and irradiance limiter.

Optical limiting now requires a sophisticated set of properties including various nonlinear materials, different physical processes, various device designs including a number of lenses and other optical devices, optical pulse shaping, and the characteristics of the laser source including wavelength, pulse duration and pulse repetition rate. This range of materials, processes, and devices involve complex optical propagation requiring a vast diversity of parameters that cannot be fully analyzed without the use of various numerical codes. Along with new materials and device structures, new numerical codes

will be key elements in the development of optical limiters. Numerical investigation will be required to make additional advances by examining the various combinations of material, physical, and device parameters that would be too time consuming and/or costly to perform in the laboratory.

Physical mechanisms used in optical limiters include nonlinear refraction, nonlinear scattering, two photon absorption, thermal nonlinearity, and reverse saturable absorption. Materials used in optical limiters include fullerenes, porphyrins, liquid crystals, carbon black and nanostructured materials [1]-[10]. Various device design and structures also play an important role. Examples of different device design include tandem and graded density structures [7].

One of the first passive limiter was developed by Leite et. al. [12] in 1967 based on the thermal lensing effect in nitrobenzene. This device regulated the output power of a continuous wave (CW) Argon ion laser. It wasn't until 1983 that CS₂ [13] was used as an optical limiting material for nanosecond pulses. The experiment used a focused geometry and showed that the mechanisms involved in limiting transmission were catastrophic self-focusing together with absorption and scattering resulting from laser induced breakdown. In the last two decades experiments and theory on optical limiting has greatly expanded with the mechanisms including two-photon absorption, excited state absorption, nonlinear refraction and nonlinear scattering. A variety of materials are being investigated and characterized to improve the performance of optical limiters. Recent research interests are focused on organic material, like dyes, liquid crystals and nanostructures, which exhibit very high nonlinearity.

The damage threshold is determined by several factors including the total energy/fluence entering the eye [14]-[19], the pulse duration [14], the spot size [16], and the number of incident pulses [15]. Ocular media are transparent in the range between 0.35 μ m to 1.3 μ m [14]. Early experiments by Birngruber et. al. [17] measured laser eye damage at the ED50 level (the 50% probability of retinal lesion development) as a function of pulse width from about 0.1 sec to about 100 fs. For pulse durations above the microsecond level (~ 20 μ s), the damage mechanism is due to thermal effects [14] and is irradiance dependent (i.e. W/cm²). In the pulse duration range from nanoseconds to microseconds (ns to ~ 20 μ s), the damage mechanism is due to thermo-acoustic effects [14]. In this region the diffusion of heat is negligible and the damage threshold is fluence dependent (i.e. J/cm²). The threshold for eye damage is ~ 0.1 J/cm². However, for ultrashort pulses (subpicosecond), the data shows lower threshold damage as the pulse width decreases. For example, the damage threshold is ~ 0.01 J/cm² for picosecond pulses. These results for ultrashort pulses (~ 100 femtoseconds) were later confirmed by additional experiments. [18]. The damage mechanism is now believed to be due to self-focusing and laser induced breakdown [19].

The damage threshold [20]-[22] also depends on the laser spot size at the retina where the diffraction limited spot size is 22 μ m. Measurements of the damage threshold [16] were performed using a flashlamp-pumped dye laser for spot sizes ranging from 22 μ m to 1400 μ m (the corresponding field of view is from 1.5mrad to 100mrad). It was observed that the damage threshold increased linearly with the diameter of the spot size in this range. However, when the spot size exceeds 1400 μ m, the damage threshold is fluence dependent, i.e. proportional to the area of the spot [16]. Most experiments are performed using single incident pulses, but multi-pulse experiments have also been performed.

Recent experiments [15] have investigated multiple exposures with repetition rates less than several kilohertz.

Indirect detectors include solid detectors, image intensifiers and infrared (IR) night vision detectors. In the IR-II and IR-III ranges the thermal emissivity of various objects is used to produce an image that is observed by an IR seeker. Several strategies are used to damage indirect detectors. For example, the lens in front of a typical solid-state detector will focus the incoming laser beam so that even a medium energy laser can damage the detector. Another technique for sensor damage involves destroying the front optics of the detection system.

The mechanism responsible for optical sensor damage also depends on the pulse duration: below 1ns, high power densities can be reached, leading to electrical breakdown; above 1ns, the damage originates from thermal effects that are fluence dependent as long as the pulse duration is shorter than the thermal time constant to become power density dependent [23].

2 Mechanisms of Optical Limiting

Optical limiting was first observed in liquids [12]-[13] where these early experiments demonstrated that the limiting could be due to self-focusing or self-defocusing as well as absorption and scattering. Later experiments showed that semiconductors have large optical nonlinearities [24]. Optical power limiting experiments conducted in CdS, GaAs, and CdSe [25] were attributed to the mechanism of two-photon absorption. Additionally, experiments in the 1960s, showed that organic dye molecules exhibited optical limiting property [26]. This was recognized as reverse saturable absorption, so-named because it is due to the large absorption cross-section of the excited state of the molecule.

During the last several years many mechanisms used for passive optical limiting include nonlinear absorption, nonlinear refraction, and induced scattering [1]-[10]. The nonlinear absorption can be due to two-photon absorption or reverse saturable absorption. Examples of nonlinear refraction are the electronic Kerr effect, the excitation of free carriers or optically induced heating. Figure 1 shows some of the time scales for the various physical phenomena.

2.1 Kerr Nonlinear Refraction

At high input energy the focal point of the beam will be shifted due to nonlinear refraction [27], therefore the energy at the detector will be limited. Because of the non-uniform distribution of the Gaussian beam profile, the nonlinear medium acts as either a positive or a negative lens depending on the sign of the nonlinear refractive index. By proper design of the aperture and lens structure, the nonlinear medium forms a lens that can increase the portion of the beam blocked by the aperture.

In a Kerr nonlinear medium, the change of index is due to 3rd order nonlinear susceptibility.

$$\Delta n_{Kerr} \cong n_2 I \quad (1)$$

For a Gaussian beam, the transverse intensity distribution is given by

$$I = I_0 \exp(-r^2/w^2) \quad (2)$$

The refractive index distribution is given by [1]

$$\Delta n = \Delta n_0 \exp(-r^2/w^2) \cong \Delta n_0 (1 - r^2/w^2) \quad (3)$$

$$\Delta n_0 = n_2 I_0$$

Another critical parameter of nonlinear refractive optical limiter is the position of the nonlinear medium in the device. The optimal position for self-focusing or self-defocusing is one Rayleigh range before or after the focus of the device, respectively which can be verified by Z-scan experiments. If the Kerr nonlinear medium also has positive dispersion then pulse splitting occurs as the pulse propagates [28]-[29]. These effects may have to be taken into account when pulse shaping is important.

2.2 Nonlinear Scattering

Carbon-black suspension (CBS) shows broadband nonlinear scattering effect [30]-[31]. The experimental data indicates that optical limiting due to CBS is fluence dependent, and effective for broadband nanosecond laser pulses. The limiting threshold of CBS is around 100W peak power. The mechanism of CBS optical limiter is simple. The microscopic-sized carbon particles are rapidly heated to 4000⁰ K by strong linear absorption, giving rise to thermionic emission, which in the presence of the strong electric field leads to avalanche ionization. The resulting microplasma then rapidly expands into the surrounding liquid and strongly scatters the incident light for the duration of the existence of the plasma (100ns). In addition, since the carbon particles are ionized during the process, the suspension must be replenished after each laser exposure.

2.3 Two Photon Absorption

Two-photon absorption (TPA) is a two-stage process; wherein, the electron is first excited to an intermediate state (whose lifetime is extremely short), followed by absorption of a second photon that excites it to the final state. The intensity of the beam along the z-axis can be obtained by solving the phase and amplitude of field separately in the Maxwell wave equation. If the excited state absorption is ignored, then the propagation of the beam intensity is given by

$$\frac{\partial I}{\partial z} = -\alpha I - \beta_2 I^2 \quad (4)$$

where α is the linear absorption coefficient and β_2 is the TPA coefficient which is related to the imaginary part of $\chi^{(3)}$, the third-order nonlinear susceptibility. The solution of Eq. (4) is

$$I(L) = \frac{I_0}{(1 + I_0 \beta_2 L)} \quad (5)$$

where linear absorption is assumed to be zero. It is easily seen that the light transmission depends on the initial intensity, TPA coefficient, and thickness of the medium. An

increase in intensity leads to a decrease in transmission. In TPA materials it is useful if the first excited state is longer than the pulse width so that each electron is excited once per pulse. However a short upper excited state is required to reduce the saturation of the excited state absorption that diminishes the limiting performance.

2.4 Semiconductor Nonlinearity

Semiconductors have broad absorption bands and are capable of producing TPA over a large wavelength range where linear absorption is low. In semiconductors electrons can be excited to the conduction band where they can contribute to the absorption. In the case of free carrier generation in semiconductors, the change of the refractive index is given by

$$\Delta n_{FC} = \frac{n_{eh}\beta_2}{2\hbar\omega} \int_{-\infty}^{\infty} I^2 dt \quad (6)$$

where n_{eh} is the index change per photo-generated carrier pair [32]-[33]. However a problem with semiconductors is that they tend to have low damage thresholds that restrict their applicability in optical limiting. The typical semiconductor is also more useful for the infrared region than the visible region.

2.5 Thermal Nonlinearity

The effects of thermal nonlinearity depend on the time scale involved. The refractive index profile of the medium changes as a light pulse passes through it due to induced temperature and density gradients. This mechanism is known as thermal lensing because the refractive index change follows the beam shape forming a lens-like structure in the medium [34]. For steady-state conditions thermal lensing is diffusion dominated [35], [36]. However density changes resulting from the temperature gradient are described by acoustic-waves because they travel at the speed of sound [37]-[39].

When the laser pulse is longer than a few microseconds the heating effect is diffusion dominated and the heating of the material is described by the diffusion equation [38]

$$\rho c_p \frac{\partial T}{\partial t} - \kappa \nabla^2 T = \alpha_L I \quad (7)$$

where ρ is the density of the medium, c_p is the specific heat at constant pressure, κ is the thermal conductivity, and $\alpha_L I$ is the portion of the laser power transformed into heat. In nanosecond region the effects of diffusion can be ignored and the induced temperature change for any spatial position is given by

$$\Delta T(t) = \frac{1}{\rho c_p} \int_0^t \alpha_L I(t') dt' \quad (8)$$

In this temporal region, the thermal effects can be described by photon-acoustic wave interaction

$$\nabla^2(\Delta n) - \frac{1}{C_s^2} \frac{\partial^2(\Delta n)}{\partial t^2} = -\frac{\gamma^e \beta}{2n} \nabla^2(\Delta T) \quad (9)$$

where C_s^2 is the velocity of sound. This expression may be simplified when the acoustic transit time is less than the pulse width and is given by

$$\Delta n \equiv \left(\frac{dn}{dT} \right)_0 \Delta T \quad (10)$$

where

$$\left(\frac{dn}{dT} \right)_0 = \frac{\gamma^e \beta}{2n} \quad (11)$$

is the thermo-optic constant. However for picosecond duration pulses both the thermal diffusion and photo-acoustic effects can be ignored.

2.6 Reverse Saturable Absorption

Reverse saturable absorption (RSA) occurs when the excited state absorption cross section (σ_{ex}) is larger than the ground state absorption cross section (σ_g). The materials involved are usually large chromophores [3]-[8]. The process is modeled by several vibronically broadened electronic energy states. In general a five level system is involved as shown in Fig. 2. The RSA material typically consists of three singlet states (ground state and two excited states) coupled with two triplet states. These materials have a large ratio of excited state to ground state absorption cross section and can achieve a large nonlinear attenuation while maintaining a high linear transmittance (>70%). In addition, RSA materials with fast singlet excited state absorption and long-lived triplet state absorption [40]-[43] can give rise to optical limiting over a wide range of pulse widths (i.e. nanoseconds to sub-picoseconds). Modifications to the molecular structure of the chromophores can lead to enhanced optical limiting in specific spectral ranges. Consequently theoretical [44]-[48] and experimental [3] studies are in progress in several laboratories.

In the simplified case [1], [7] the transmission through the RSA materials is described by the fluence (F) equation given by

$$F(L) = \frac{F(0) \exp(-\alpha L)}{1 + (\sigma_{ex} \alpha / 2\hbar\omega) F(0) L_{eff}}, \quad (12)$$

$$L_{eff} = (1 - \exp(-\alpha L)) / \alpha$$

where $F(0)$ is the incident fluence. Similar to the TPA process, the transmittance of RSA depends on the incident fluence, excited states absorption cross-section, linear absorption coefficient and effective thickness.

3. RSA Materials

A number of materials are used for optical limiting such as fullerenes, porphyrins, phthalocyanine, naphthalocyanines and neutral nickel dithiolenes [6]. Some of the main optical limiting candidates are described next.

3.1 Fullerenes-Carbon 60 / Carbon 70

Carbon 60 (C60) has excited-state absorption greater than the ground state from ~400 to 900nm, which covers the entire visible spectrum. Therefore C60 is a broadband optical limiting material [49]-[57]. Due to a long triplet excited-state lifetime $>40\mu\text{s}$, C60 can protect against pulse duration of hundreds of microseconds pulses. The performance of C60 optical limiter also depends on host materials [49], e.g. toluene solution, polymethyl methacrylate (PMMA) and solid xerogel matrices.

Carbon 70 (C70) has a smaller ratio of excited-state to ground state absorption and a higher threshold for optical limiting [52], [53]. In the visible wavelength range, C70 has stronger absorption than C60 because of the reduced symmetry of C70 relative to C60 and a lower triplet state quantum yield. Therefore C60 and C70 have different clamping intensities and the limited output intensities. The values of the mixture C60/C70 solution are higher than that of C60 solutions and lower than that of C70 solutions. Variable limited output intensity can be obtained by changing the C70 content in the solution of C60/C70 mixture or the concentration of the solution [51].

3.2 Porphyrin and related derivatives

Optical limiting in porphyrin-based materials was first reported in 1985 [6]. Thereafter an extensive range of porphyrins and their expanded family have been intensively studied [58]-[73]. Figure 4 shows a basic porphyrin structure. To date the largest ratio of excited-state to ground-state cross section absorption reported is about a factor of 45 at 532nm [58] in tetra (trimethylsilyl) ethynyl porphyrin (TTMSAP(Pb)). Preliminary work shows porphyrins with closed-shell metal atoms have relatively long excited state lifetimes. A recent halogenation study shows that bromine atoms substituted in porphyrins [59] increase the triplet yield via the heavy atom effect and decrease the triplet lifetime. One molecular design strategy is to maintain a planar and symmetric structure to ensure that the spectra of linear absorption features are narrow. Ab initio electronic structure calculations are used to examine the structures, excited state spectra, and ionization potentials of porphyrins [6], [44]-[48].

Recent experimental work has shown that heavy central atoms, halogens, and electron donating groups in porphyrins can enhance RSA and optical limiting. However, the mechanisms involved in enhancing optical limiting are not understood. Nguyen et al.[60] studied the effects of zinc and halogens in porphyrins, in order to examine their possible role in enhancing RSA, using ab initio electronic structure calculation and configuration interaction method using single substitutions (CIS) calculation. The CIS calculations examined the effect of the central metal and β -halogenation on the electronic spectra of porphyrins. Their calculation of excitation energy agrees well with experiments. Thus these computational methods may provide an approach for modeling the properties of optical limiters on a molecular scale [60].

4 General five level model for RSA

4.1 Rate equations

The well-known phenomenological rate equations [6] describing the electronic state populations for the five-state model are

$$\partial N_0 / \partial t = -\sigma_{01} I N_0 / \hbar \omega_0 + k_{10} N_1 + k_{30} N_3 \quad (13)$$

$$\partial N_1 / \partial t = \sigma_{01} I N_0 / \hbar \omega_0 - (\sigma_{12} I / \hbar \omega_0 + k_{10} + k_{13}) N_1 + k_{21} N_2 \quad (14)$$

$$\partial N_2 / \partial t = \sigma_{12} I N_1 / \hbar \omega_0 - k_{21} N_2 \quad (15)$$

$$\partial N_3 / \partial t = -(\sigma_{34} I / \hbar \omega_0 + k_{30}) N_3 + k_{13} N_1 + k_{43} N_4 \quad (16)$$

$$\partial N_4 / \partial t = \sigma_{34} I N_3 / \hbar \omega_0 - k_{43} N_4 \quad (17)$$

where N_p is the electron number density of the state p , σ_{pq} is the absorption cross-section for electron pumping from the state p to the state q and k_{pq} is the decay rate from the state p to the state q . The assignment of the electron densities, N_p , in Fig. 2(e) is as follows: N_0 corresponds to the ground level of the singlet state, S_0 ; N_1 corresponds to the first excited level of the singlet state, S_1 ; N_2 corresponds to the second excited level of the singlet state, S_2 ; N_3 corresponds to the first excited level of the triplet state, T_1 ; and N_4 corresponds to the second excited level of the triplet state, T_2 . In these materials, the total number, N_T , of electrons is conserved such that $N_0 + N_1 + N_2 + N_3 + N_4 = N_T$. The initial population is given by $N_0 = N_T$ and $N_1 = N_2 = N_3 = N_4 = 0$.

4.2 Intensity Equations

The optical pulse has an intensity I with angular frequency ω_0 , and \hbar is Planck's constant. Using a density matrix approach, we [74]-[77] obtained the induced electric polarization vector from the dipole moment perturbation calculation for the RSA material and reduced the general propagation equation in our model to an equation for the pulse intensity that is in agreement with previous results. This reduced propagation equation for the pulse intensity is given by

$$\frac{dI}{dz} = -[\sigma_{01} N_0 + \sigma_{12} N_1 + \sigma_{34} N_4] I. \quad (18)$$

To date most studies of RSA have been experimental, with a few theoretical studies using the reduced intensity model. More complete theoretical studies, including propagation effects, are needed in order to guide, validate and reduce the number of experiments.

For most applications, the RSA material is contained in a matrix substrate. In certain cases, the matrix substrate can exhibit Kerr nonlinearity and material dispersion. The polarization vector for this material can be expressed as

$$P = P_L + P_{NL}, \quad (19)$$

where P_L is the linear polarization vector and P_{NL} is the nonlinear polarization vector. The nonlinear polarization term can be written as

$$P_{NL} = \epsilon_0 \epsilon_{NL} E, \quad (20)$$

where E is the electromagnetic field and ϵ_{NL} is the nonlinear contribution to the dielectric constant. It is described by

$$\epsilon_{NL} = \frac{3}{4} \chi_{xxxx}^{(3)} |E|^2, \quad (21)$$

where $\chi_{xxxx}^{(3)}$ is the third order susceptibility. The index of refraction contains both a linear frequency dependent term and a nonlinear intensity dependent term defined by

$$n(\omega, |E|^2) = n(\omega) + \tilde{n}_2 |E|^2, \quad (22)$$

$$\tilde{n}_2 = \frac{3}{8n_0} \text{Re}(\chi_{xxxx}^{(3)})$$

The electromagnetic field $E(r, z, t)$ propagating in a matrix substrate containing the RSA material is written in terms of a slowly varying envelope $A(r, z, t)$ and the carrier frequency ω_0 of the electromagnetic field, such that

$$E(r, z, t) = A(r, z, t) e^{ik_0 z - i\omega_0 t} + c.c. \quad (23)$$

Using the slowly varying envelope approximation, we obtain the equation for propagation of the electromagnetic field in the matrix substrate containing the RSA material [74]-[75]

$$\begin{aligned} i \left[\frac{\partial}{\partial z} + k_1 \frac{\partial}{\partial t} \right] A(z, r, t) + \frac{1}{2k_0} \nabla_{\perp}^2 A(z, r, t) - \frac{1}{2} k_2 \frac{\partial^2}{\partial t^2} A(z, r, t) + \left[\frac{\tilde{n}_2 \omega_0}{c} |A|^2 \right] A(z, r, t) \\ + \frac{i}{2} \left[\sigma_{01} N_0(z, t, |A|^2) + \sigma_{12} N_1(z, t, |A|^2) + \sigma_{34} N_3(z, t, |A|^2) \right] A(z, r, t) = 0 \end{aligned} \quad (24)$$

where $\nabla_{\perp}^2 = \frac{\partial^2}{\partial r^2} + \frac{1}{r} \frac{\partial}{\partial r}$, $k_n = \frac{\partial^n k}{\partial \omega^n} \Big|_{\omega_0}$, and the last term describes the RSA material whose intensity dependence is given in Eqs. (13-17). Equation (18), in the absence of diffraction, dispersion and Kerr nonlinearity, reduces to the intensity equation. It should be noted that the Kerr nonlinearity is real and conserves energy. In the absence of RSA, but together with anomalous dispersion, the Kerr nonlinearity can give rise to localized solitary waves and solitons. However, the RSA nonlinearity is pure imaginary and leads to an intensity dependent energy loss. Because of their nonlinear dependence on intensity, RSA materials behave very differently than linear absorbers. Their ideal feature is the ability to transmit low intensity light, but absorb high intensity light.

We assume an incident pulse of the form, $A(r, 0, t) = A_0 \exp\left(\frac{-r^2}{2a_0^2}\right) \exp\left(\frac{-t^2}{2T_0^2}\right)$, where a_0 is the spatial beam waist, T_0 is the 1/e half-width of the temporal intensity, and A_0^2 is the incident peak intensity. We use the transformation [75],

$$Q = \frac{A}{A_0}, \rho = \frac{r}{a_0}, \xi = \frac{z}{k_0 a_0^2}, \tau = \frac{(t - k_1 z)}{T_0}, \quad (25)$$

to obtain the non-dimensioned equation

$$\left[i \frac{\partial}{\partial \xi} + \frac{1}{4} \nabla_\rho^2 - \frac{1}{2} \gamma \frac{\partial^2}{\partial \tau^2} \right] Q(\xi, \rho, \tau) + ap |Q(\xi, \rho, \tau)|^2 Q(\xi, \rho, \tau) \\ + i \delta \left[\sigma_{01} N_0(\xi, \tau, |Q|^2) + \sigma_{12} N_1(\xi, \tau, |Q|^2) + \sigma_{34} N_3(\xi, \tau, |Q|^2) \right] Q(\xi, \rho, \tau) = 0 \quad (26)$$

coupled to the rate equations

$$\begin{pmatrix} \dot{N}_0 \\ \dot{N}_1 \\ \dot{N}_2 \\ \dot{N}_3 \\ \dot{N}_4 \end{pmatrix} = \begin{pmatrix} -\hat{\sigma}_{01} & k_{10} & 0 & k_{30} & 0 \\ \hat{\sigma}_{01} & -(\hat{\sigma}_{12} + k_{10} + k_{13}) & k_{21} & 0 & 0 \\ 0 & \hat{\sigma}_{12} & -k_{21} & 0 & 0 \\ 0 & k_{13} & 0 & -(\hat{\sigma}_{34} + k_{30}) & k_{43} \\ 0 & 0 & 0 & \hat{\sigma}_{34} & -k_{43} \end{pmatrix} \begin{pmatrix} N_0 \\ N_1 \\ N_2 \\ N_3 \\ N_4 \end{pmatrix} \quad (27)$$

where $ap = \left(\frac{1.22\pi}{4}\right)^2 \frac{\tilde{n}_2 \omega_0 A_0^2 k_0 a_0^2}{c} \cdot \gamma = \frac{a_0^2 k_0 k_2}{2T_0^2}$, $\delta = \frac{a_0^2 k_0}{2}$, $\hat{\sigma}_{pq} = \sigma_{pq} A_0^2 |Q|^2 / \hbar \omega_0$, and

\dot{N} denotes differentiation with respect to time. Equations (26) and (27) represent the set of coupled equations that must be solved numerically.

The numerical procedure combines a split step beam propagation method for the dispersive terms with a finite-difference method for the diffractive terms. The nonlinear terms are treated in the time domain. The numerical solution is solved in the form

$$\begin{aligned}
\frac{\partial Q}{\partial \xi} &= (D_{DS} + D_{DF} + NL)Q, \\
D_{DS} &= -i \frac{\gamma}{2} \frac{\partial^2}{\partial \tau^2}, \\
D_{DF} &= \frac{i}{4} \nabla_\rho^2, \\
NL &= NL_1 + NL_2 \\
NL_1 &= iap|Q|^2 \\
NL_2 &= -\delta \left[\sigma_{01} N_0(\xi, \tau, |Q|^2) + \sigma_{12} N_1(\xi, \tau, |Q|^2) + \sigma_{34} N_3(\xi, \tau, |Q|^2) \right]
\end{aligned} \tag{28}$$

where D_{DS} (D_{DF}) is the dispersion (diffraction) operator, NL_1 describes the Kerr nonlinearity operator and NL_2 describes the nonlinear absorption operator resulting from the RSA material. For the symmetrical split beam method (BPM), we write the equation as

$$Q(\xi + \Delta\xi) = e^{\frac{\Delta\xi}{2} D_{DS}} e^{\frac{\Delta\xi}{2} D_{DF}} e^{\frac{\Delta\xi}{2} NL_1} e^{\int_\xi^{\xi+\Delta\xi} NL_2(\xi') d\xi'} e^{\frac{\Delta\xi}{2} NL_1} e^{\frac{\Delta\xi}{2} D_{DF}} e^{\frac{\Delta\xi}{2} D_{DS}} Q(\xi), \tag{29}$$

where the integral is approximated by

$$\int_\xi^{\xi+\Delta\xi} NL_2(\xi') d\xi' \cong \frac{\Delta\xi}{2} [NL_2(\xi + \Delta\xi) + NL_2(\xi)]. \tag{30}$$

5. Numerical Method

A schematic diagram of the numerical code processes is given in Fig. 3. Some of the material parameters include the cross-sections for absorption ($\sigma_{01}, \sigma_{12}, \sigma_{34}$), the decay rates for the five-level model ($k_{10}^{-1}, k_{21}^{-1}, k_{13}^{-1}, k_{43}^{-1}, k_{30}^{-1}$), the carrier concentration, the Kerr nonlinear coefficient, the 2-photon absorption coefficient, the group velocity dispersion, the linear index of refraction and linear absorption. Many of these parameters can be varied in the numerical calculations to optimize the performance and compared with ab initio quantum molecular calculations to guide molecular modeling. Examples of input optical beam parameters include pulse intensity, width, radius, shape, and repetition rate. Analysis of the output files can identify any changes in pulse reshaping that may affect nonlinear transmission. In other words, pulse reshaping such as self-focusing or defocusing or temporal compression or expansion may result in beneficial optical limiting results. Some device parameters include the number of lens and their focal length and distance from each object and the number of elements in the optical limiter. The numerical calculations can be used to optimize the device design and thus minimize the number of costly experiments that have to be performed.

The numerical procedure combines the split step beam propagation method for the dispersive terms and the finite-difference method for the diffractive terms. The nonlinear terms are treated in the time domain. Numerical calculations are performed with non-dimensional equations.

5.1 Numerical Method and Operator Equations

The mathematical terms [74]-[76] are evaluated using a discrete space and time grid given by $\tau \rightarrow \tau_i$, $\xi \rightarrow \xi_n$, $\rho \rightarrow \rho_j$ and the field can be written in the shorthand notation, $Q_{i,j}^n$. The dispersion and diffraction terms are calculated in the frequency domain using the fast Fourier transform method; however, the nonlinear terms are calculated in the time domain.

In the frequency domain, the dispersion operator becomes

$$\tilde{D}_{DS}(\omega) = \frac{i\gamma\omega^2}{2}. \quad (31)$$

The linear diffraction term is given by

$$\frac{\partial Q}{\partial \xi} = \kappa \nabla_\rho^2 Q(\xi, \rho, \omega), \quad \kappa = \frac{i}{4}. \quad (32)$$

This term is solved by the finite-difference scheme,

$$\frac{\partial Q}{\partial \xi} = \frac{Q_{i,j}^{n+1} - Q_{i,j}^n}{\Delta \xi}, \quad (33)$$

and the Crank-Nicholson method

$$\begin{aligned} \nabla_\rho^2 Q = & \frac{1}{\rho_j} \frac{1}{4\Delta\rho} [Q_{i,j+1}^{n+1} - Q_{i,j-1}^{n+1} + Q_{i,j+1}^n - Q_{i,j-1}^n] \\ & + \frac{1}{2(\Delta\rho)^2} [Q_{i,j+1}^{n+1} - 2Q_{i,j}^{n+1} + Q_{i,j-1}^{n+1} + Q_{i,j+1}^n - 2Q_{i,j}^n + Q_{i,j-1}^n] \end{aligned} \quad (34)$$

$$\Delta\rho = \rho_{j+1} - \rho_j$$

for $0 < \rho_j < \rho_{\max}$.

Combining Eqs. (33) and (34), the field at $\Delta\xi/2$ is given by

$$\begin{aligned} \frac{\kappa}{\Delta\rho} \frac{\Delta\xi}{2} \left(\frac{1}{2\rho_j} - \frac{1}{\Delta\rho} \right) Q_{i,j-1}^{n+1} + \left(\frac{\kappa \Delta\xi}{(\Delta\rho)^2} + 1 \right) Q_{i,j}^{n+1} - \frac{\kappa}{\Delta\rho} \frac{\Delta\xi}{2} \left(\frac{1}{2\rho_j} + \frac{1}{\Delta\rho} \right) Q_{i,j+1}^{n+1} = \\ - \frac{\kappa}{\Delta\rho} \frac{\Delta\xi}{2} \left(\frac{1}{2\rho_j} - \frac{1}{\Delta\rho} \right) Q_{i,j-1}^n - \left(\frac{\kappa \Delta\xi}{(\Delta\rho)^2} - 1 \right) Q_{i,j}^n + \frac{\kappa}{\Delta\rho} \frac{\Delta\xi}{2} \left(\frac{1}{2\rho_j} + \frac{1}{\Delta\rho} \right) Q_{i,j+1}^n \end{aligned} \quad (35)$$

However at $\rho=0$,

$$(1+\varphi)Q_{i,0}^{n+1} - \varphi Q_{i,1}^{n+1} - (1-\varphi)Q_{i,0}^n - \varphi Q_{i,1}^n = 0, \quad (36)$$

$$\varphi = \frac{2\kappa \Delta\xi}{\rho_1}$$

At the maximum radial value, ($\rho = \rho_{\max} = \rho_N$) we obtain

$$\theta Q_{i,N-1}^{n+1} + (1-\theta)Q_{i,N}^{n+1} + \theta Q_{i,N-1}^n - (1+\theta)Q_{i,N}^n = 0, \quad (37)$$

$$\theta = \frac{\kappa \Delta\xi}{2\rho_N(\rho_N - \rho_{N-1})}$$

Using Eqs. (35)-(37), Eq. (33) is written in the form

$$\Xi_1(\omega_i) \bullet \vec{q}_i^{n+1} = \Xi_2(\omega_i) \bullet \vec{q}_i^n, \quad (38)$$

$$\vec{q}_i^n = (Q_{i,0}^n, \dots, Q_{i,j}^n, \dots, Q_{i,N}^n)$$

and Ξ_1 and Ξ_2 are tri-diagonal matrices. The matrix Ξ_1 is composed of the sub-diagonal, diagonal and super-diagonal elements,

$$\begin{aligned} \vec{a}(\omega_i) &= \left[0, \dots, \frac{\kappa \Delta\xi}{\rho_{j+1} - \rho_{j-1}} \left\{ \frac{1}{2\rho_j} - \frac{1}{\rho_j - \rho_{j-1}} \right\}, \dots, \theta \right], \\ \vec{b}(\omega_i) &= \left[1 + \varphi, \dots, \frac{\kappa \Delta\xi}{\rho_{j+1} - \rho_{j-1}} \left\{ \frac{1}{\rho_{j+1} - \rho_j} + \frac{1}{\rho_j - \rho_{j-1}} \right\}, \dots, 1 - \theta \right], \\ \vec{c}(\omega_i) &= \left[-\varphi, \dots, -\frac{\kappa \Delta\xi}{\rho_{j+1} - \rho_{j-1}} \left\{ \frac{1}{2\rho_j} + \frac{1}{\rho_{j+1} - \rho_j} \right\}, \dots, 0 \right] \end{aligned} \quad (39)$$

and the matrix Ξ_2 is composed of the sub-diagonal, diagonal and super-diagonal terms

$$\begin{aligned}
\bar{d}(\omega_i) &= \left[0, \dots, -\frac{\kappa \Delta \xi}{\rho_{j+1} - \rho_{j-1}} \left\{ \frac{1}{2\rho_j} - \frac{1}{\rho_j - \rho_{j-1}} \right\}, \dots, -\theta \right], \\
\bar{e}(\omega_i) &= \left[1 - \varphi, \dots, 1 - \frac{\kappa \Delta \xi}{\rho_{j+1} - \rho_{j-1}} \left\{ \frac{1}{\rho_{j+1} - \rho_j} + \frac{1}{\rho_j - \rho_{j-1}} \right\}, \dots, 1 + \theta \right], \\
\bar{f}(\omega_i) &= \left[\varphi, \dots, \frac{\kappa \Delta \xi}{\rho_{j+1} - \rho_{j-1}} \left\{ \frac{1}{2\rho_j} + \frac{1}{\rho_{j+1} - \rho_j} \right\}, \dots, 0 \right]
\end{aligned} \tag{40}$$

5.2 Propagation Equation

The propagation including the RSA nonlinearity is more complex because of the coupling between the propagation equation and the rate equations. The propagation term for the RSA is written as the coupled set of equations

$$\frac{\partial Q}{\partial \xi} = -\delta(\sigma_{01}N_0 + \sigma_{12}N_1 + \sigma_{34}N_3)Q, \tag{41}$$

$$\frac{\partial}{\partial \tau} \tilde{N}(\xi, \tau, |Q|^2) = \hat{M}(\xi, \tau, |Q|^2) \tilde{N}(\xi, \tau, |Q|^2), \tag{42}$$

The propagation can be expressed as

$$Q_i^{n+1} = \exp\left[-\delta \frac{\Delta \xi}{2} (\sigma N)\right] Q_i^n, \tag{43}$$

$$\begin{aligned}
\sigma N &= \sigma_{01} \left[N_0(\xi_{n+1/2}, \tau_{i-1/2}) + N_0(\xi_{n+1/2}, \tau_{i+1/2}) \right] \\
&\quad + \sigma_{12} \left[N_1(\xi_{n+1/2}, \tau_{i-1/2}) + N_1(\xi_{n+1/2}, \tau_{i+1/2}) \right] \\
&\quad + \sigma_{34} \left[N_3(\xi_{n+1/2}, \tau_{i-1/2}) + N_3(\xi_{n+1/2}, \tau_{i+1/2}) \right]
\end{aligned} \tag{44}$$

However, the N 's must be determined from the rate equation, and depend on the intensity $|Q|^2$. The rate equations can be solved in matrix form as

$$\frac{\tilde{N}(\xi_{n+1/2}, \tau_{i+1/2}) - \tilde{N}(\xi_{n+1/2}, \tau_{i-1/2})}{\Delta \tau} = \hat{M} \frac{1}{2} [\tilde{N}(\xi_{n+1/2}, \tau_{i+1/2}) + \tilde{N}(\xi_{n+1/2}, \tau_{i-1/2})] \tag{45}$$

Collecting like terms gives the matrix expression

$$\tilde{N}(\xi_{n+1/2}, \tau_{i+1/2}) = \left[1 - \frac{\Delta \tau}{2} \hat{M} \right]^{-1} \left[1 + \frac{\Delta \tau}{2} \hat{M} \right] \tilde{N}(\xi_{n+1/2}, \tau_{i-1/2}), \tag{46}$$

expanding the inverse matrix and keeping terms to second order,

$$\bar{N}(\xi_{n+1/2}, \tau_{i+1/2}) \equiv \left[1 + \Delta\tau \hat{M} + (\Delta\tau \hat{M})^2 / 2 \right] \bar{N}(\xi_{n+1/2}, \tau_{i-1/2}). \quad (47)$$

Equation (47) is used in the propagation equation.

6. Results and Conclusions

The following sections highlight the main results and conclusions.

6.1 Initial Results

Some initial results are described in this section. Figure 4 shows the pulse energy as a function of space and time for an incident energy of 10 μJ at four propagation distances ($z=0.28$ cm, 0.57 cm, 0.86 cm, and 1.15 cm). The pulse shapes are plotted as functions of time and radius, and the contour plot of the pulse is given at the top of each pulse shape. The negative (positive) times correspond to the leading (trailing) edge of the pulse. It can be seen from Fig. 4, that the trailing edge of the pulse becomes less steep as the pulse propagates and the peak of the pulse advances in time relative to the moving coordinate frame. For plotting purposes the pulses are normalized to a height of one unit. For convenience the values of the peak energy at each propagation distance is given in Fig. 4. These values show the decrease in energy as the pulse propagates. While the overall pulse shape exhibits small changes as it propagates, the energy decreases rapidly. An example of the carrier density is shown in Fig. 5. For convenience, the carrier densities are normalized by the expression

$$\begin{aligned} n_0 + n_1 + n_2 + n_3 + n_4 &= 1.0, \\ n_l &= N_l / N_T \end{aligned} \quad (48)$$

where $l = 0, 1, 2, 3, 4$ and the initial condition of the carrier density before the incidence of the pulse is $n_0=1.0$ and $n_1=n_2=n_3=n_4=0$. In all cases it was found that the value of n_4 was negligible; therefore, it was not included in the plots with the other carrier densities. Figure 5 shows plots of the carrier densities at $z=0.28$ cm. The maximum values of the carrier densities are given in the figure caption as well as the minimum value for n_0 . The minimum value for all other n 's is zero, so it is not necessary to indicate their values. Initially the entire carrier population is in S_0 (i.e. $n_0=1.0$), but as the leading edge of the pulse enters the RSA material, carriers are excited from the ground state (S_0) to the first excited state (S_1). Because the entire carrier density is originally in S_0 , the pulse absorption is determined by the product $\sigma_{01}n_0I$ at the leading edge of the pulse. As the first excited state becomes populated (i.e. $n_1>0$), the absorption of the pulse is determined by the relationship $(\sigma_{01}n_0 + \sigma_{12}n_1)I$. The population of the second excited state (i.e. n_2) decays very rapidly because $k_{21}^{-1} < \tau_0$. The decay rates k_{10}^{-1} and $k_{13}^{-1} > \tau_0$ so the first excited state (i.e. S_1) can maintain some population (i.e. $n_1>0$) for a time greater than τ_0 . However, as shown in Fig. 5, there is minimal decay to the triplet state T_1 . Therefore, even though σ_{34} is about the same size as σ_{12} , there is little population of T_2 (i.e. $n_4 \sim 0$) which is verified by the numerical calculations. Because S_1 remains populated for a time greater than τ_0 , the trailing edge of the pulse intensity experiences greater absorption

than the leading edge, thus causing the peak of the pulse to move forward in time relative to the moving frame.

Figure 6 shows the pulse energy as a function of space and time for an incident energy of 500 μJ . In this case, new details of the pulse propagation behavior are observed using the space and time dependent code. Initially strong carrier depletion occurs at the center of the pulse resulting in a slower decay for the peak energy. This behavior is in contrast with the previous results shown in Fig. 4. In order to investigate the origin of this behavior the pulse shapes are plotted at four propagation distances (the same distances used in Fig. 4). Figure 6 shows a new lobe developing on the leading edge of the pulse ($z=0.57$ cm). As the pulse propagates the high intensity region is absorbed by the material leading to pulse splitting at $z=1.15$ cm. Figure 7 shows the carrier densities at $z=0.28$ cm. The leading edge of the pulse excites the carriers from the ground state (S_0) to the first excited state (S_1). However because of the high pulse energy, S_0 is almost completely depleted (i.e. n_0 decreases to a minimum value of $\sim 10^{-4} \approx 0$). At the leading edge of the pulse, the carrier density is increased to the first excited state S_1 (i.e. $n_1 > 0$). However at the center of the pulse the energy is sufficient to populate the second excited state S_2 (i.e. n_2 reaches a maximum value of ~ 0.8). This maximum population of S_2 occurs only near the pulse center because the decay rate for this state is faster than the temporal pulse width. In fact, this rapid population and depopulation of S_2 actually results in a depletion of n_1 near the pulse center as shown by the contour plot of n_1 in Fig. 7. However, the trailing edge of the pulse still has sufficient energy to create significant population of S_1 (i.e. n_1 reaches a maximum value of 0.987 for temporal values corresponding to the trailing edge of the pulse) as shown in Fig. 7. The decay rate from S_1 to S_0 is longer than the temporal pulse width so S_1 does not decay rapidly. The state T_1 is not heavily populated because of the relatively long decay rate of S_1 to T_1 . (n_3 reaches a maximum value of $\sim 10^{-2}$) Numerical calculations show that $n_4 \approx 0$. As the pulse propagates ($z=0.57$ cm) through the RSA material a temporal lobe forms on the leading edge of the pulse as shown in Fig. 6. This temporal lobe is caused by the complex interplay between the pulse intensity, absorption cross-sections and decay rates of S_1 and S_2 . As the pulse propagates to $z=0.86$ cm, the higher intensity portion of the pulse is reduced relative to the lobe on the leading edge because of stronger absorption. The carrier density remains mostly in S_0 because the intensity at this distance is only 0.018 which is not sufficient enough to cause much carrier excitation. Then as the pulse propagates to $z=1.15$ cm temporal splitting develops because the trailing edge of the pulse has been more strongly absorbed owing to its greater intensity.

6.2 Three Distinctive Regions

Numerically we observed three distinct regions: (1) linear absorption due to carrier excitation from the ground state to the first excited state; (2) limiting region due to carrier excitation from the first excited state to the second excited state; and (3) saturation region at high incident energy. In the linear region (low incident energy < 10 uJ) the absorption is due to the ground state to the first excited singlet state and there is a symmetric reduction in the pulse shape. This region is not shown here due to limitations of space. Figure 8 shows the 2-D and 3-D intensity and carrier density plots in the limiting region (50 uJ). Part (I) of this figure shows the 2-D plots of the pulse Intensity and the carrier

density; and part (II) shows the 3-D plots of the carrier densities. In this case, the absorption is due to the transition from the first excited singlet state to the second excited singlet state leading to greater absorption. The leading edge of the pulse excites the carriers from the ground state to the first excited state and the trailing edge of the pulse is absorbed by the carrier excitation from the first excited state to the second excited state. As a result, most absorption occurs in the trailing edge of the pulse resulting in a temporal shift of the pulse toward the leading edge.

Figure 9 shows the 2-D and 3-D intensity and carrier density plots in the saturation region (1000 uJ). Part (I) of this figure shows the 2-D plots of the pulse intensity and the carrier density; and part (II) shows the 3-D plots of the carrier densities. At high input energy (~1000 uJ) the carriers are excited to the second excited state at the leading edge of the pulse resulting in less absorption during the pulse duration; thereby, increasing the transmission as the input energy increases.

Further numerical results show that variation of the material parameters such as the decay rates, the cross section of absorption of the material, and initial carrier density, in addition to the pulse properties such as the pulse width and spatial width can enhance the limiter performance. Therefore a detailed microscopic understanding of the pulse and the carrier densities in each of the three physical regions is required to describe the dynamics of limiter behavior.

6.3 Propagation Through RSA Material in Kerr Medium

In general the RSA material is embedded in a matrix substrate, which may exhibit the Kerr nonlinearity. This nonlinearity may lead to self-focusing of the light beam as it propagates through the material. Figure 10 shows a plot of the transmission as a function of the coefficient of the Kerr nonlinearity and demonstrates that self-focusing can enhance the nonlinear absorption of the RSA material. Because the linear absorption is quite significant in the RSA material much of the laser energy is absorbed before significant self-focusing can occur. Therefore we investigate the effects of a two layer absorber in which the first layer exhibits the Kerr nonlinearity and the second layer exhibits RSA absorption. First we describe various pulse shaping techniques.

6.4 Pulse shaping techniques

Examples of pulse shaping with nonlinearity are shown in Figs. 11, 12 and 13. Pulse shaping techniques include reshaping the pulse in the time domain i.e. pulse compression or pulse broadening and reshaping in the spatial domain i.e. self-focusing of self-defocusing.

6.5 Spatial pulse shaping: Self-focusing

It has been noted previously that for RSA limiters, the material is placed in a focal plane. However this can be cumbersome for some applications. Another approach involves using a Kerr nonlinear medium before the RSA material to self-focus the light.

Figure 16 shows the use of a Kerr nonlinear medium to self-focus light into a RSA tandem limiter. Figure 11 shows change in transmission in an optical limiter when a Kerr nonlinear medium is used before the nonlinear absorber material. This figure shows the transmission as a function of incident energy.

6.6 Temporal pulse shaping techniques

In the time domain, pulse shaping can be accomplished by using Kerr nonlinearity and GVD (negative GVD leads to pulse compression and positive GVD leads to pulse expansion). For example, pulse shaping may be used before the RSA material in order to change nanosecond/microsecond pulses to picosecond pulses or vice versa. This can then be used to take advantage of the decay rates and kinetics of the RSA material. Additionally certain detectors may be more sensitive to broad temporal pulses and some may be more sensitive to short temporal pulses. Thus pulse reshaping using passive nonlinearity in a tandem optical limiter may provide a significant advantage that would not be possible without the Kerr nonlinear/dispersive medium.

6.7 Self-focusing and RSA

The effects of the combination of self-focusing and RSA are shown in Figs. 14-16. The input parameters are $T_0 = 4.0$ ps, $R_0 = 45\mu\text{m}$, $\Lambda = 532$ nm and carrier density $= 6.0322 \times 10^{-4} \text{ nm}^{-3}$. Figure 14 shows the pulse compression after one-diffraction length in a Kerr nonlinear medium where the peak intensity increases by a factor of 18. Figure 15 shows the propagation of the compressed optical pulse in 0.7 mm of RSA material. It shows the depletion of the ground singlet state and the population of the second excited singlet state. There is very little population of the triplet state. Figure 16 shows an increase in absorption when self-focusing is used to precede the RSA material. This material acts as a nonlinear lens.

6.8 Multiple Pulses

Substantial efforts have been used to investigate transmission for various optical limiters using a single incident pulse. However, lasers often produce a train of pulses. We investigated numerically the effects of multiple pulses and pulse separation. The input condition for multiple pulses is given by

$$Q(0, \tau) = \sum_{k=0}^N \sqrt{E_0} \exp\left[-\left(\tau - k\tau_r\right)^2 / 2\tau_0^2\right] \quad (49)$$

where τ_r is the pulse separation and E_0 is the pulse energy. Figure 17 shows a schematic diagram of the multiple pulses. Figure 18 shows the transmission curve for a train of seven pulses as a function of input energy for pulse separations of $\tau_r = 2$ and 10. Our results show that for closely spaced pulses ($\tau_r = 2$) there is a reduction in transmission in the region of excited-state absorption.

Detailed analysis of the pulse shapes indicate that this effect is due to pulse coalescence that results in increased input energy. Figure 19 shows 2-D and 3-D plots of

the pulse train intensity for seven incident pulses. Fig. (a) and (b) show the pulse train before the excited-state material. Fig. 19(b) shows that the seven incident pulses have merged into five pulses and their peak energy has increased by about 60%. Fig. 19 (c) and (d) show the pulse train after transmission through the excited-state material. The first pulse in the train excites carriers to the excited state absorption level; however, the carriers do not have sufficient time to return to the ground state before the next pulse arrives. Eventually, an equilibrium state among the carrier densities is achieved such that the trailing pulses reach constant transmission energy.

We also investigated the pulse shapes for the case of large pulse separation ($\tau_r = 10$). Figure 20 shows 2-D and 3-D plots of the pulse train intensity for seven incident pulses. Fig. (a) and (b) show the pulse train before the excited-state material. Fig. 20(b) shows that the seven incident pulses do not merge and their peak energy does not increase. Therefore Fig. 1 shows greater transmission for this input energy than for the closely spaced pulse train. Fig. 20(c) and (d) show the pulse train after transmission through the excited-state material. Again, the first pulse in the train excites carriers to the excited state absorption level but the carriers do not have sufficient time to return to the ground state before the next pulse arrives. This leads to nearly constant transmission energy for the trailing pulses.

We have numerically investigated the effects of multiple pulses on excited-state optical limiters. For closely spaced pulses, pulse interactions leads to enhanced peak energy and improved limiting behavior. However, even for widely spaced pulses, the trailing pulses reach a near constant, but lower, transmission energy. Our initial results show that transmission of pulse trains behave differently than transmission of a single pulse. Since many lasers produce pulse trains or are externally modulated to produce pulse trains, the effects of multiple pulses on optical limiting are of increased importance.

7.0 Conclusions

Increasing usage of high power lasers in laboratory research, measurement, medical treatment and weapons make human eyes and other optical imaging/detecting systems more vulnerable to laser related damage. Laser induced detector damage such as electron breakdown in semiconductor detectors or condensed media, thermal acoustic explosion and thermal chemical reaction in the retina can happen when the detector is illuminated by a very high irradiance laser beam directly or indirectly (through some kind focusing optical structure). An effective optical limiting device can prevent or reduce damage by clamping the excessive energy and power from these high intensity light sources.

Nonlinear properties including nonlinear refractive, absorption and scattering make passive optical limiting possible. Over the last several decades, many materials have been discovered that exhibit optical limiting properties. These materials include semiconductors (TPA), carbon-black suspension (thermal scattering), fullerenes (RSA), and porphyrins (RSA). Currently porphyrins and their derivatives are considered by many to be very promising materials.

The nonlinear mechanisms used for optical limiting have different properties that require various models. For example, nonlinear scattering in CBS is fluence dependent with broadband features, Kerr nonlinearity and two-photon absorption are intensity

dependent and occur instantaneously, while the nonlinear absorption in RSA material can be fluence or intensity dependent and depends on pulse width and beam shape.

One of the key features to the successful design of optical limiting is numerical simulation. The increasing complexity of the materials, device geometry, and optical beam shaping and signal processing necessitates the use of numerical simulation for system optimization. In an optical limiting system using RSA material, the propagation equations are coupled to the rate equation. The mathematical methods used for optical limiter calculations include the Huygen-Fresnel Principle, the Crank-Nicholson finite difference method, the spectral or Fourier transform method and the split-step method.

The effects of spatiotemporal behavior in optical limiting systems have only recently been addressed. However, these phenomena could potentially play a significant role in optical limiting. For example, in the eye, pulse compression due to nonlinear Kerr effect and negative GVD may reduce the damage threshold; whereas, the Kerr effect and positive GVD may increase the damage threshold in the subpicosecond region. Until recently, calculations have not included the effects of both nonlinear Kerr effect and dispersion. The nonlinear Kerr effect and diffraction may have significant effects on the optical limiting system. Self-focusing can change the focal point in the system. Additionally self-focusing can shift the focal point to the exit plane of the nonlinear absorbing material and increase its optical limiting property by utilizing all of the molecules in the optical path.

Though some optical limiters have already been used in real applications, they are still insufficient to protect very sensitive devices, like human eyes, from very high-energy beams. New materials with high nonlinearity and fast response will remain a key research area. Additionally investigations on the interplay and synergism between different types of nonlinear optical phenomena may significantly improve the performance of optical limiting systems. New applications of these optical limiting materials will also be an interesting area.

BIBLIOGRAPHY

- [1] L. W. Tutt and T. F. Boggess, "A review of optical limiting mechanisms and devices using organics, fullerenes, semiconductors and other materials," *Prog. Quantum. Elect.*, vol. 17, pp.299-338, 1993.
- [2] J. A. Hermann and J. Staromlynska, "Special issue on optical limiters, switches and discriminators," *J. Nonlinear Opt. Phys. and Materials*, vol. 2, 1993.
- [3] F. Kajzar, "Proceedings of First International Workshop on Optical Power Limiting, Cannes, France" in *Nonlinear Optics, Principles, Materials, Phenomena, Devices*, Gordon & Breach, 1998.
- [4] R. Crane, K. Lewis, E. W. Van Stryland, and M. Khoshnevisan, *Materials for Optical Limiting*, vol. 374, Materials Research Society, Boston, 1994.
- [5] R. Sutherland, R. Pachter, P. Hood, D. J. Hagan, K. Lewis, and J. Perry, *Materials for Optical Limiting II*, vol. 479, Materials Research Society, San Francisco, 1997.
- [6] J. W. Perry, "Organic and metal-containing reverse saturable absorbers for optical limiters," in *Nonlinear Optics of Organic Molecules and Polymers*, H. S. Nalwa and S. Miyata, Ed. Boca Raton, FL: CRC, 1997, pp.813-839.
- [7] E. W. Van Stryland, D. J. Hagan, T. Xia, and A. A. Said, "Application of nonlinear optics to passive optical limiting," in *Nonlinear Optics of Organic Molecules and Polymers*, H. S. Nalwa and S. Miyata, Ed. Boca Raton, FL: CRC, 1997, pp. 841-860.
- [8] D. J. Hagan, "Optical limiting," in *Handbook of Optics, vol. IV*, M. Bass, J. M. Enoch, E. W. Van Stryland, and W. L. Wolfe, Eds. New York, NY: McGraw Hill, 2001, pp. 19.1-19.16.
- [9] L. Brzozowski and E. H. Sargent, "Nonlinear distributed-feedback structures as passive optical limiters," *J. Opt. Soc. Am. B*, vol.17, no.8, pp.1360-1365, 2000.
- [10] E. W. Van Stryland, M. J. Soileau, S. Ross and D. J. Hagan, "Passive Optical Limiting: Where are we?," *Nonlinear Opt.*, vol.21, pp.29-38, 1999.
- [11] V. Grolier-Mazza, "The specification of laser protection," *Nonlinear Opt.*, vol. 21, pp.78-88, 1999.
- [12] R. C. C. Leite, S. P. S. Porto and T. C. Damen, "The thermal lens effect as a power-limiting device," *Appl. Phys. Lett.*, vol. 10, no.3, pp.100-101, 1967.
- [13] M. J. Soileau, W. F. Williams, N. Mansour, E. W. Van Stryland, "Laser-induced damage and the role of self-focusing," *Opt. Eng.*, vol. 28, no.10, pp. 71-82, 1989.
- [14] D. H. Sliney, "Retinal Injury from Laser Radiation," *Nonlinear Opt.*, vol. 21, pp.1-17, 1999.
- [15] C. P. Cain, C. A. Toth, G. D. Noojin, D. J. Stolarski, R. J. Thomas, B. A. Rockwell, "Theshold for retinal injury from multiple near-infrared ultrashort laser pulses," *Health Phys.*, vol.82, no.6, pp.855-862, 2002.

- [16] J. A. Zuclich, D. J. Lund, P. R. Edsall, R. C. Hollins, P. A. Smith, B. E. Stuck and L. N. McLin, "Experimental study of the variation of laser-induced retinal damage threshold with retinal image size," *Nonlinear Opt.*, vol. 21, pp.19-28, 1999.
- [17] R. Birngruber, C. A. Puliafito, A. Gawande, W. Lin, R. W. Schoenlein, "Femtosecond Laser-Tissue Interactions: Retinal Injury Studies," *IEEE J. Quantum. Elect.*, vol. 23, no.10, pp.1836-1843, 1987.
- [18] B. A. Rockwell, D. X. Hammer, R. A. Hopkins, D. J. Payne, C. A. Toth, W. P. Roach, J. J. Druessel, P. K. Kennedy, R. E. Amnotte, B. Eilert, S. Phillips, G. D. Noojin, D. J. Stolarski, and C. Cain, "Ultrashort laser pulse bioeffects and safety," *J. Laser Appl.*, vol. 11, pp.42-44, 1999.
- [19] Q. Feng, J. V. Moloney, A. C. Newell, E. M. Wright, K. Cook, P. K. Kennedy, D. X. Hammer, B. A. Rockwell, and C. R. Thompson, "Theory and simulation on the threshold of water breakdown induced by focused ultrashort laser pulses," *IEEE J. Quantum. Elect.*, vol. 33, no.2, pp.127-137, 1997.
- [20] American National Standards Institute, Safe Use of Lasers, American National Standard Z-136.1-1993, Laser Institute of America, Orlando, FL, 1993.
- [21] American Conference of Governmental Industrial Hygienists, "Threshold Limit values for Chemical Substances and Physical Agents for 1998", Cincinnati, ACGIH, 1998. International Commission on Non-Ionizing Radiation Protection, "Guidelines on limits for laser radiation of wavelengths between 180 nm and 1,000 nm", *Health Physics*, vol. 71, no. 5, pp. 804-819, 1996.
- [22] International Commission on Non-Ionizing Radiation Protection, "Guidelines on limits for laser radiation of wavelengths between 180 nm and 1, 00 nm," *Health Physics*, vol. 71, no. 5, pp. 804-819, 1996.
- [23] P. K. Kennedy, S. A. Boppart, D. X. Hammer, B. A. Rockwell, G. D. Noojin, and W. P. Roach, "A first-order model for computation of laser-induced breakdown thresholds in ocular and aqueous media: part II-comparison to experiment," *IEEE J. Quantum. Elect.*, vol. 31, no.12, pp.2250-2257, 1995.
- [24] T. F. Bogess, S. C. Moss, I.W. Boyd, and A. L. Smirl, "Nonlinear optical energy regulation by nonlinear refraction and absorption in silicon," *Opt. Lett.* vol. 9, pp. 291-293, 1984.
- [25] J. M. Ralston and R. K. Chang, "Optical limiting in semiconductors," *Appl. Phys. Lett.*, vol.15, no.6, pp.164-166, 1969.
- [26] C. R. Giuliano and L. D. Hess, "Nonlinear absorption of light optical saturation of electronic transitions in organic molecules with high intensity laser radiation," *IEEE. J. Quantum Electron.*, vol. QE-3, pp.338-352, 1967.
- [27] J. H. Marburger, "Self-focusing: Theory," *Prog. Quantum Electron.*, vol. 4, pp. 35-110, 1975.
- [28] J. Rothenburg, "Pulse splitting during self-focusing in normally dispersive media," *Opt. Lett.*, vol. 17, no. 8, pp. 583-582, 1992.
- [29] P. Chernev and V. Petrov, "Self-focusing of light pulses in the presence of normal group-velocity dispersion," *Opt. Lett.*, vol. 17, no.3, pp.172-174, 1992.
- [30] K. Mansour, M. J. Soileau and E. W. Van Stryland, "Nonlinear optical properties of carbon-black suspensions (ink)," *J. Opt. Soc. Am. B*, vol.9, no.7, pp. 1100-1109, 1992.

- [31] D. J. Hagan, S. Yang, C. Basanez, E. W. Van Stryland, W. Moreshead and J-L. Nogués, "Optical limiting via nonlinear scattering with sol gel host materials," Proc. SPIE Power-Limiting Materials and Devices, vol. 3798, Oct. 1999, pp.17-21.
- [32] E. W. Van Stryland, Y. Y. Wu, D. J. Hagan, M. J. Soileau and K. Mansour, "Optical limiting with semiconductors", J. Opt. Soc. Am. B, vol.5, no.9, pp.1980-1989, 1988.
- [33] E. W. Van Stryland, H. Vanherzeele, M. A. Woodall, M. J. Soileau, A. L. Smirl, S. Guha, and T. F. Boggess, "Two photon absorption, nonlinear refraction, and optical limiting in semiconductors," Opt. Eng., vol.24, no.4, pp.613-623, 1985.
- [34] S. A. Akhmanov, D. P. Krindach, A. V. Migulin, A. P. Sukhorukov, and R. V. Khokhlov, "Thermal self-action of laser beams" IEEE J. Quantum. Electron., vol. QE4, pp. 568-575, 1968.
- [35] J. N. Hayes, "Thermal blooming of laser beams in fluids," Appl. Opt., vol. 11, pp.455-461, 1972.
- [36] S. J. Sheldon, L. V. Knight, and J. M. Thorne, "Laser-induced thermal lens effect: a new theoretical model," Appl. Opt., vol. 21, pp. 1663-1669, 1982.
- [37] P. R. Longaker and M. M. Litvak, "Perturbation of the refractive index of absorbing media by a pulsed laser beam," J. Appl. Phys., vol. 40, pp. 4033-4041, 1969.
- [38] G. Liu, "Theory of the photoacoustic effect in condensed matter," Appl. Opt. vol. 21, pp. 95-960, 1982.
- [39] B. L. Justus, A. J. Campillo, and A. L. Huston, "Thermal-defocusing/scattering optical limiter," Opt. Lett., vol. 19, pp. 673-675, 1994.
- [40] P. Feneyrou, "Broadband optical limiting using tandem filters with multiphoton absorber and reverse saturable absorbers," J. Nonlinear Opt. Phys. Mater., vol. 9, no. 4, pp. 523-530, 2000.
- [41] D. J. Harter, M. L. Shand and Y. B. Band, "Power/energy limiter using reverse saturable absorption," J. Appl. Phys., vol. 56, no.3, pp. 865-868, 1984.
- [42] E. W. Van Stryland, M. Sheik-Bahae, A. A. Said and D. J. Hagan, "Characterization of nonlinear absorption and refraction in advanced materials," Proc. SPIE Nonlinear optical properties of advanced materials, vol.1852, Los Angeles, CA, Jan. 20- 21, 1993, pp.135-150.
- [43] J. W. Perry, K. Mansour, I. Y. S. Lee, X. L. Wu, P. V. Bedworth, C. T. Chen, D. Ng, S. R. Marder, P. Miles, T. Wada, M. Tian, and H. Sasabe, "Organic optical limiters with a strong nonlinear absorptive response," Science, vol. 273, pp. 1533-1540, 1996.
- [44] R. Pachter, R. L. Crane, and W. W. Adams, "The design of candidate optical limiters," Proc. Mat. Res. Soc. Symp., vol. 374, pp.39-44, 1995.
- [45] K. A. Nguyen and R. Pachter, "Photoinduced hydrogen atom transfer of free-base porphyrin", J. Phys. Chem. A, vol.104, pp. 4549-4552, 2000.
- [46] K. A. Nguyen, P. N. Day and R. Pachter, "Ground and triplet excited structures and spectroscopic properties of halogenated zinc meso-tetraphenylporphyrin," J. Phys. Chem. A, vol.103, pp. 9378-9382, 1999.

- [47] K. A. Nguyen and R. Pachter, "Ground state electronic structures and spectra of zinc complexes of porphyrin, tetraazaporphyrin, tetrabenzoporphyrin, and phthalocyanine: A density function theory study," *J. Chem. Phys.*, vol. 114, no.24, pp. 10757-10767, 2001.
- [48] K. A. Nguyen, P. N. Day and R. Pachter, "Triplet excited states of free-base porphyrin and its β -octahalogenated derivatives," *J. Phys. Chem. A*, vol.104, pp.4748-4754, 2000.
- [49] A. Kost, M. B. Klein, T. K. Dougherty and W. E. Elias, "Optical limiting with C60 in polymethyl methacrylate," *Opt. Lett.* vol. 18, no.5, pp. 334-338, 1993.
- [50] F. Lin, J. Zhao, T. Luo, M. Jiang, Z. Wu and Y. Xie, "Optical limitation and bistability in fullerenes," *J. Appl. Phys.*, vol. 74, no.3, pp. 2140-2142, 1993.
- [51] Y. Sun, Q. Gong, S. Yang, Y.H. Zou, L. Fei, X. Zhou and D. Qiang, "Optical limiting properties of buckminsterfullerene," *Optics Commun.*, vol.102, pp. 205-207, 1993.
- [52] L. W. Tutt and A. Kost, "Optical limiting performance of C60 and C70 solutions," *Nature*, vol.356, pp. 225-226, 1992.
- [53] J. E. Wray, K. C. Liu, C. H. Chen, W. R. Garrett and M. G. Payne, "Optical power limiting of fullerenes," *Appl. Phys. Lett.*, vol. 64, no.21, pp.2785-2787, 1994.
- [54] J. R. Heflin, D. Marciu, C. Figura, S. Wang, P. Burbank, S. Stevenson, H. C. Dorn and J. C. Withers, "Degenerate Four-Wave Mixing in Endohedral Metallofullerenes and Optical Limiting of C60 Derivatives and Higher Fullerenes," *Proc. SPIE Fullerenes and Photonics III*, vol. 2854, Dec. 1996, pp.162-173.
- [55] S. Foley, M. N. Berberan-Santos, A. Fedorov, R. V. Bensasson, S. Leach and B. Gigante, "Effect of halogenated compounds on the photophysics of C70 and a monoadduct of C70: Some implications on optical limiting behaviour", *Chem. Phys.*, vol.263, pp.437-447, 2001.
- [56] J. Barroso, A. Costela, I. Garcia-Moreno and J. L. Saiz, "Wavelength dependence of the nonlinear absorption of C60- and C70- toluene solutions," *J. Phys. Chem. A*, vol.102, no.15, pp.2527-2532, 1998.
- [57] B. Honerlage, J. Schell and R. Levy, "Optical limiting in C60 doped solid sol-gel glasses," *Nonlinear Opt.*, vol. 21, pp. 189-200, 1999.
- [58] K. J. McEwan, J. M. Roberson and H. L. Anderson, "Porphyrin dye media for optical limiting," *Mat. Res. Soc. Symp. Proc.*, vol. 797, pp. 395-406, 2000.
- [59] W. Sun, C. C. Byeon, M. M. McKerns, C. M. Lawson, G. M. Gray and D. Wang, "Optical limiting performances of asymmetric pentaazadentate porphyrin-like cadmium complexes," *Appl. Phys. Lett.*, vol.73, no.9, pp.1167-1169, 1998.
- [60] K. A. Nguyen, P. N. Day and R. Pachter, "DoD Challenge Application: New Materials Design," *Proc. High Performance Computing (HPC) 98*, pp. 63-68, 1998.
- [61] D. J. Hagan, T. Xia, A. A. Said, T. H. Wei and E. W. Van Stryland, "High dynamic range passive optical limiters," *International J. Nonlinear Opt. Phys.* vol.2, no.4, pp.483-502, 1993.

- [62] M. Brunel, F. Chaput, S. A. Vinogradov, B. Campagne and M. Canva, "Reverse saturable absorption in palladium and zinc tetraphenyltetraenzoporphyrin doped xerogels" *Chem. Phys.*, vol.218, pp.301-307, 1997.
- [63] D. V. G. L. N. Rao, F. J. Aranda, J. F. Roach and D. E. Remy, "Third-order nonlinear optical interactions of some benzoporphyrins," *Opt. Lett.*, vol. 58, no.12, pp. 1241-1242, 1991.
- [64] W. Su, T. M. Cooper, N. Tang, D. Krein, H. Jiang, D. Brandelik, P. Fleitz, M. C. Brant and D. G. McLean, "Structure-optical property relationships of porphyrins," *Mat. Res. Soc. Symp. Proc.* vol. 479, pp. 313-318, 1997.
- [65] F. J. Aranda, D. V. G. L. N. Rao, B. R. Kimball, B. S. DeCrisofano, M. Nakashima, J. A. Akkara, D. J. Tarantolo and Y. Y. Hsu, "Optical power limiting in solid state porphyrin polycarbonate composites," *Proc. SPIE Nonlinear Optical Liquids and Power Limiters*, vol.3146, Birmingham, Al, July 1997, pp.176-185.
- [66] W. Blau, H. Byrne, W.M. Dennis and J.M. Kelly, "Reverse saturable absorbtion in tetraphenylporphyrins," *Optics Commun.*, vol.56, no.1, pp. 25-29, 1985.
- [67] G. L. Wood, M. J. Miller and A. G. Mott, "Investigation of tetrabenzoporphyrin by the Z-scan technique" *Opt. Lett.*, vol. 20, no.9, pp. 973-975, 1995.
- [68] J. Si, M. Yang, Y. Wang, L. Zhang, C. Li, D. Wang, S. Dong, W. Sun, "Nonlinear absorption in metallo-porphyrin-like," *Optics Communications*, vol.109, pp.487-491, 1994.
- [69] R. Bonnett, A. Harriman and A. N. Kozyrev, "Photophysics of halogenated porphyrins," *J. Chem. Soc. Faraday Trans.*, vol.88, no.6, pp.763-766, 1992.
- [70] S. W. McCahon, L. W. Tutt, M. B. Klein and G. C. Valley, "Optical limiting with reverse saturable absorbers," *Proc. SPIE Electro-Optical Materials for Switches, Coatings, Sensor Optics, and Detectors*, vol.1307, Oct. 1990 pp.304-314.
- [71] W. Su, T. M. Cooper, K. Nguyen, M. C. Brant, D. Brandelik and D. G. McLean, "Structure-optical property relationships of porphyrins," *Proc. SPIE Nonlinear Optical Liquids for Power Limiting and Imaging*, vol.3472, Oct. 1998, pp. 136-143.
- [72] D. J. Hagan, E. Miesak, R. Negres, S. Ross, J. Lim and E. W. Van Stryland, "Nonlinear spectrometry of chromophores for optical limiting," *Proc. SPIE Nonlinear Optical Liquids for Power Limiting and Imaging*, vol.3472, Oct. 1998, pp. 80-90.
- [73] W. Su, T. M. Cooper and M. C. Brant, "Investigation of Reverse-Saturable absorption in brominated porphyrins," *Chem. Mater.*, vol.10, pp.1212-1213, 1998.
- [74] M. J. Potasek, "Optical Limiting Materials, Phenomena, Devices, and Numerical Simulations: An Overview", *Optics and Quantum Electronics*, 2004, in press.
- [75] S. Kim, M. J. Potasek and D. McLaughlin "Propagation of the Electromagnetic Field in Optical Limiting Reverse Saturable Absorbers", *Phys. Rev A*, 61, 25801, 2000.

- [76] M.J. Potasek, S. Kim, D. McLaughlin, "All Optical Power Limiting" J. Nonlinear Optical Physics and Materials, special issue: Optical Limiters, Switches, and Discriminators: Materials, Principles and Devices, vol.9, pp. 343-364, 2000.
- [77] M. J. Potasek and S. Kim, "Spatio-Temporal Self-Focusing and Dispersion of High Bandwidth Optical Pulses", 2000 OSA Annual Meeting/ILS-XVI Tech. Digest., RI, Oct. 22-26, 2000, p. 110.

Appendix

Publications

"Analysis of Femtosecond Multiphoton Processes Involved in Microfabrication, Micro/nano Structures and Sensors", Y. Gao and M. J. Potasek, submitted to IEEE Journal Quantum Electronics.

"Large Nonlinear Optical Properties of Semiconductor Quantum Dot Arrays Embedded in an Organic Medium", Y. Gao, N. Q. Huong, J. Birman and M. J. Potasek, submitted to Journal Applied Physics.

"Optical Limiting Materials, Phenomena, Devices, and Numerical Simulations: An Overview", M. J. Potasek, Optics and Quantum Electronics, 2004, in press.

"Analysis of Pulse Shaping and Carrier Concentration Changes in the Linear, Excited State and Saturation Regions of Excited State Absorbers", M. Potasek, submitted to Opt. Lett.

"All Optical Power Limiting", **invited paper**, M.J. Potasek, S. Kim, D. McLaughlin, J. Nonlinear Optical Physics and Materials, special issue: Optical Limiters, Switches, and Discriminators: Materials, Principles and Devices, vol.9, pp. 343-364 (2000).

"Propagation of the Electromagnetic Field in Optical Limiting Reverse Saturable Absorbers", S. Kim, M. J. Potasek and D. McLaughlin, Phys. Rev A, 61, 25801 (2000).

Conference Publications

"Highly Effective Thin Film Optical Filter Constructed of Semiconductor Quantum Dot 3D Arrays in an Organic Host", Y. Gao, N. Q. Huong, J. Birman and M. J. Potasek, Proc. Photonics East, 2004 accepted.

"Detailed Simulation of Two-Photon Absorption for 3D Micro-Nano Engineering and Patterning", Y. Gao and M. J. Potasek, Photonics East, 2004 accepted.

"Optical Limiting for Novel High Bandwidth Optical Networks", **invited paper and best paper award**, Proc. International Conference on Computer, Communication and Control Technologies CCCT '03 and the 9th International Conference on Information Systems Analysis and Synthesis ISAS '03, vol. VI, eds. H. W. Chu, J. Ferrer, D. Reisis and E. Hansen, July 31- Aug. 1-2, 2003, Orlando, FL, pp. 315-320.

"Numerical Simulations and Modeling for Optical Limiting Materials and Structures with Applications in Laser Protection", M. J. Potasek, Proceedings IEEE Sarnoff Symposium, March 2003.

"Optical Processing in Free Space Using Ultrashort Pulses", M. J. Potasek and S. Kim, CLEO Tech Digest, May 6-11, 2001, Baltimore, MD, paper CTuM38, p. 181.

"Spatio-Temporal Self-Focusing and Dispersion of High Bandwidth Optical Pulses", M. J. Potasek and S. Kim, 2000 OSA Annual Meeting/ILS-XVI Tech. Digest., RI, Oct. 22-26, 2000, p. 110.

Presentations

M. J. Potasek, S. Kim, D. McLaughlin, "Propagation in Reverse Saturable Absorbers", Proc. Nonlinear Optics Mtg., Tucson, AZ, Sept. 2001.

M. J. Potasek, "From Megabits to Terabits: Nonlinear Optics At the Frontier of Laser Protection, Information Processing, and Ocular Biomedicine", **invited talk**, City College of New York, NY, Nov. 2001.

M. J. Potasek, "Excited State Absorbers: Effects of Multiple Pulses on Optical Limiters", Annual Optical Society Meeting, Nov. 2003.

M. J. Potasek, "Novel Arrays of Nanostructured Semiconductor Organic Materials with Large Third Order Nonlinearity", City College of New York, N.Y., Oct. 2003.

M. J. Potasek, "Numerical Simulations and Modeling for Optical Limiting Materials and Structure", IEEE Symposium, The College of New Jersey, March 2003.

Technical Reports

"Enhanced User Interface and Visualization of Data for the Numerical 3-D Optical Nonlinear Propagation and Rate Equations", M. J. Potasek, Technical Report, 2002.

"Numerical Algorithms for Propagation In Nonlinear Kerr and Reverse Saturable Absorber Materials with Dispersion and Diffraction", S. Kim and M. J. Potasek, Technical Report, 2002.

"Description of Numerical Simulations for Optical Limiting Materials and Structures", M. J. Potasek, Technical Report, 2002.

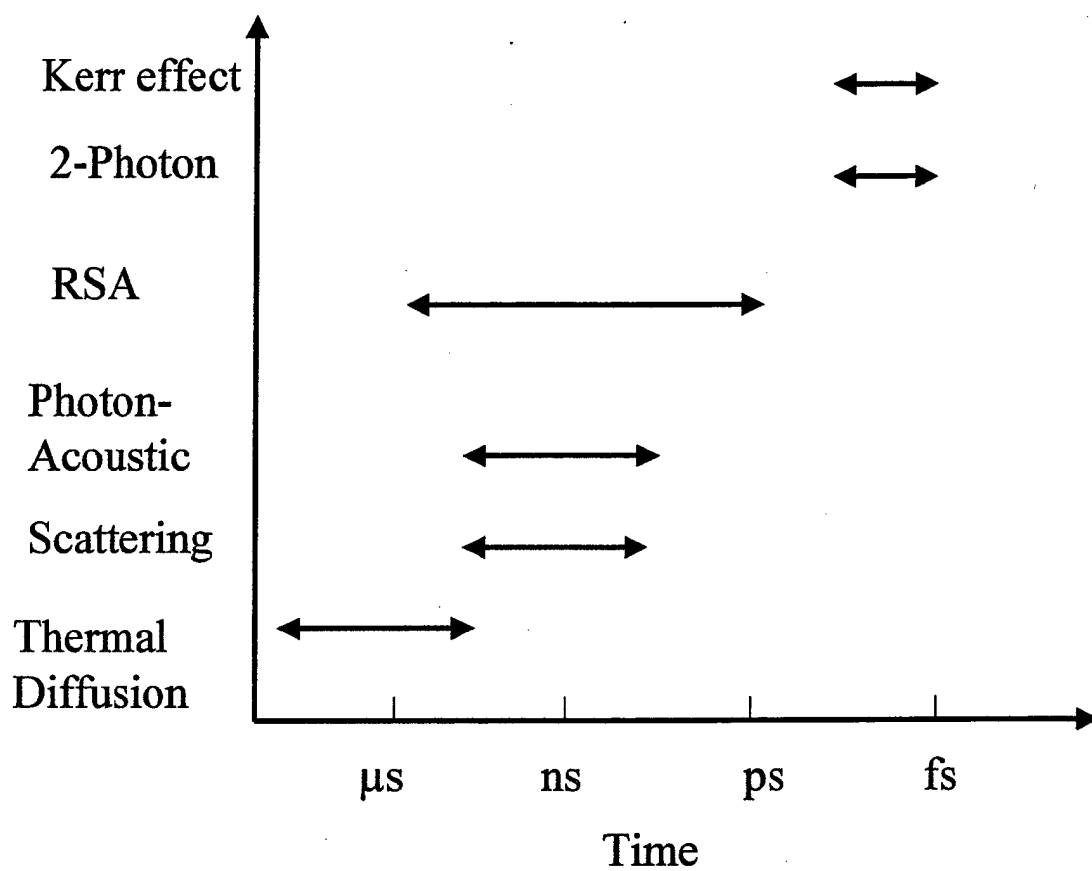


Fig.1. Schematic of approximate time scales for various optical limiting phenomena.

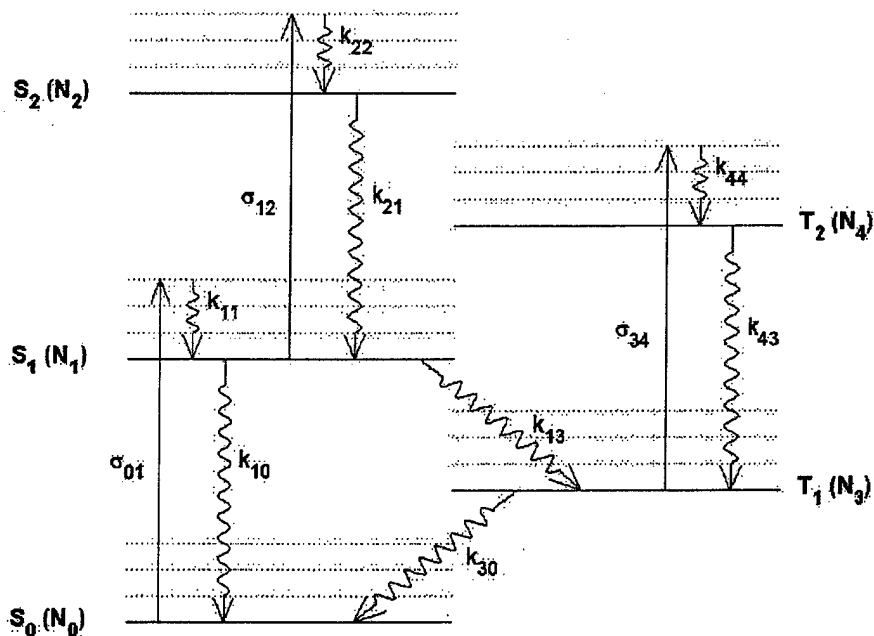


Fig. 2. Schematic energy level for a chromophore. The electronic states are represented by solid horizontal lines and the vibronic states are represented by dotted horizontal lines. S_q represents a singlet state and T_q represents a triplet state. The photon absorption excitations are represented by solid vertical lines, and the decay processes are represented by wavy lines. The absorption coefficients σ_{pq} and the decay constants k_{pq} are described in the text. The physical values used for our calculations are: $\sigma_{01}=2.4 \times 10^{-18} \text{ cm}^2$, $\sigma_{12}=3.0 \times 10^{-17} \text{ cm}^2$, $\sigma_{34}=4.8 \times 10^{-17} \text{ cm}^2$, $k_{10}=0.144 \text{ ns}^{-1}$, $k_{21}=1.0 \text{ ps}^{-1}$, $k_{13}=77.8 \text{ } \mu\text{s}^{-1}$, $k_{30}=50.0 \text{ ms}^{-1}$, $k_{43}=1.0 \text{ ps}^{-1}$, and k_{11}, k_{22}, k_{33} are due to vibrational decays which are assumed to be instantaneous.

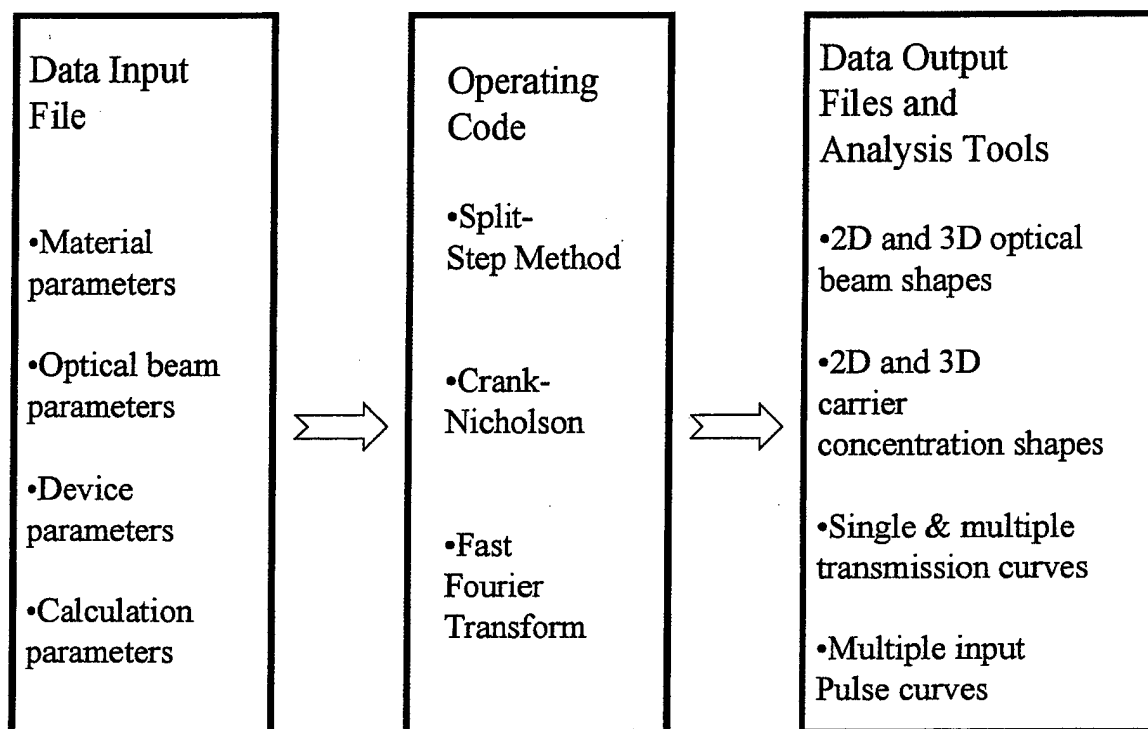
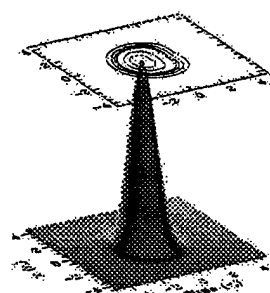
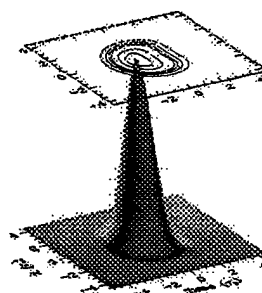


Fig. 3. Diagram of the features of the numerical beam propagation code.

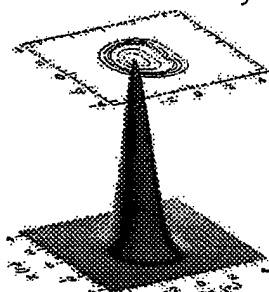
Pulse Propagation (Incident Energy=10 μ J)



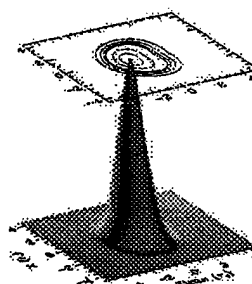
Z=0.28 cm
Peak=0.26, Total=0.40



Z=0.57 cm
Peak=0.13, Total=0.22



Z=0.86 cm
Peak=0.085, Total=0.15



Z=1.15 cm
Peak=0.045, Total=0.075

Fig. 4. Pulse shapes of the laser beam at four propagation distances. The incident energy is 10 μ J and the carrier density $N_T=6.022 \times 10^{17} \text{ cm}^{-3}$.

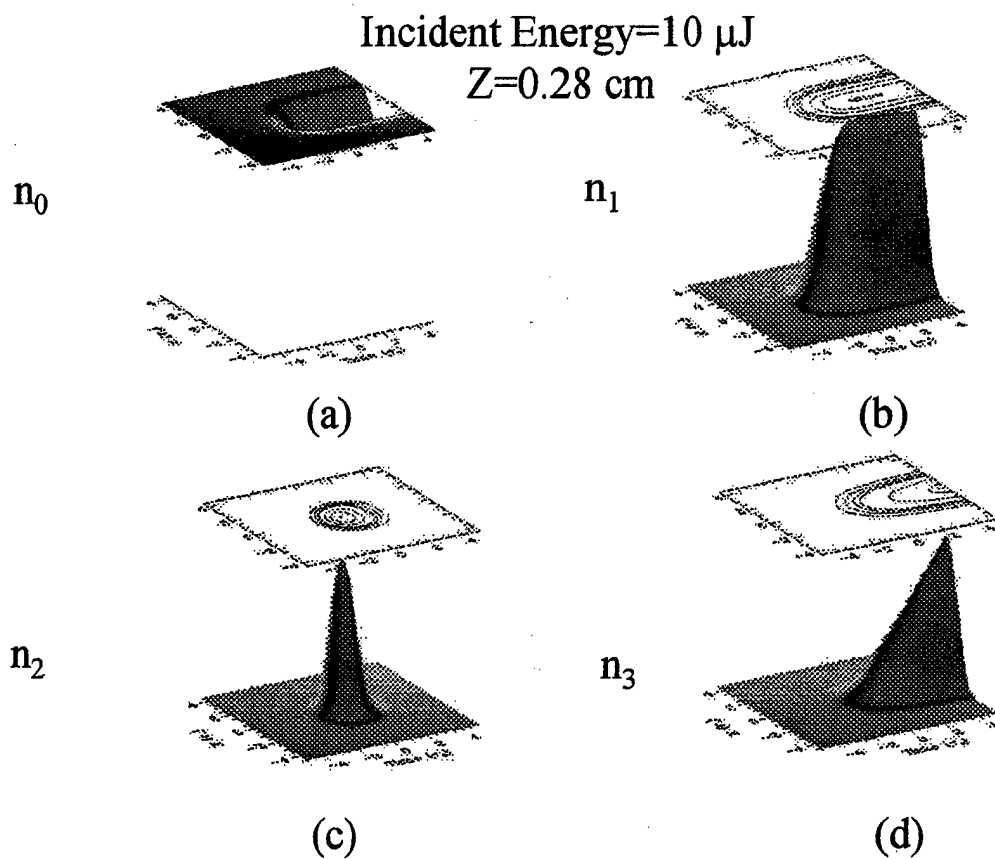
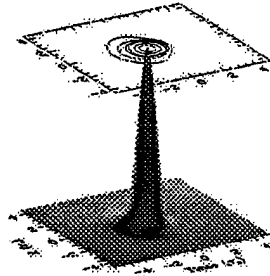
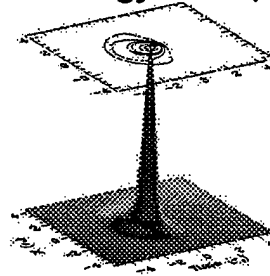


Fig. 5. Carrier densities as a function of space and time. (a) Ground state: Maximum value = 1.0 and minimum value = 0.772; (b) First excited state of single state: Maximum value = 0.226; (c) Second excited state of single state: Maximum value = 0.00624; (d) First state of the triplet state: Maximum value = 0.00466.

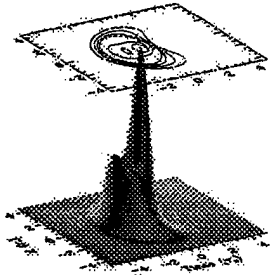
Pulse Propagation (Incident Energy=500 μJ)



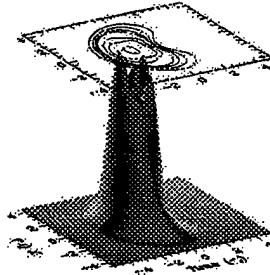
$Z=0.28$ cm
Peak=0.45, Total=0.18



$Z=0.57$ cm
Peak=0.15, Total=0.04



$Z=0.86$ cm
Peak=0.014, Total=0.018



$Z=1.15$ cm
Peak=0.002, Total=0.007

Fig. 6. Pulse shapes of the laser beam at four propagation distances. The incident energy is 500 μJ and the carrier density $N_T=6.022 \times 10^{17} \text{ cm}^{-3}$.

Incident Energy=500 μ J, Z=0.28 cm

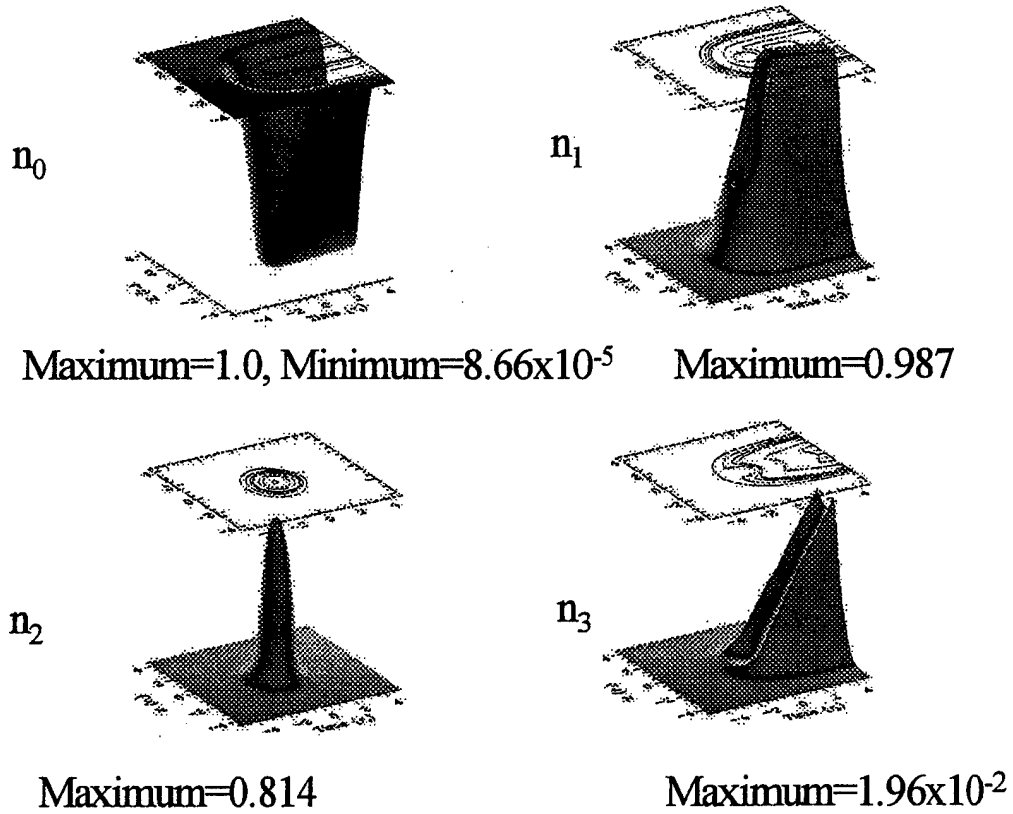
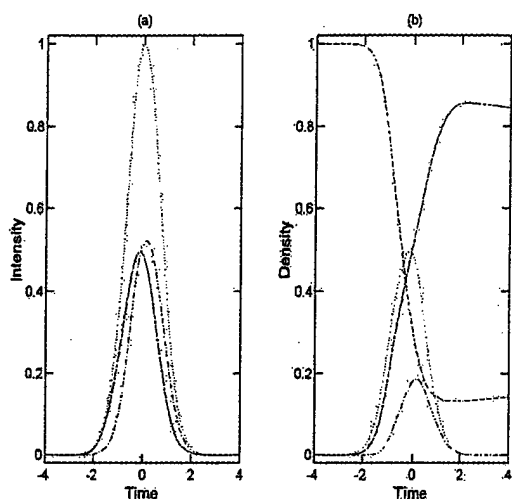
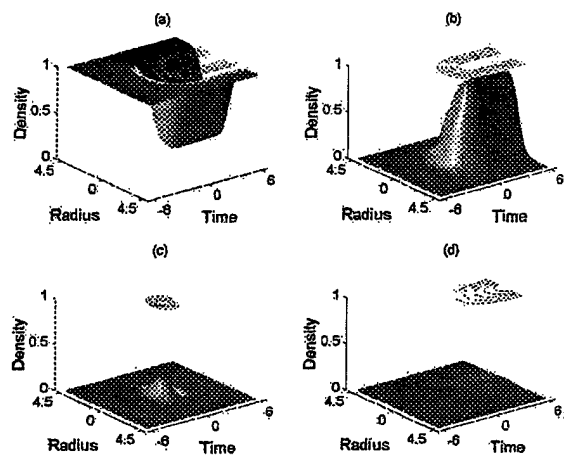


Fig. 7. The carrier densities at $z=0.28$ cm and incident energy $=500 \mu\text{J}$.

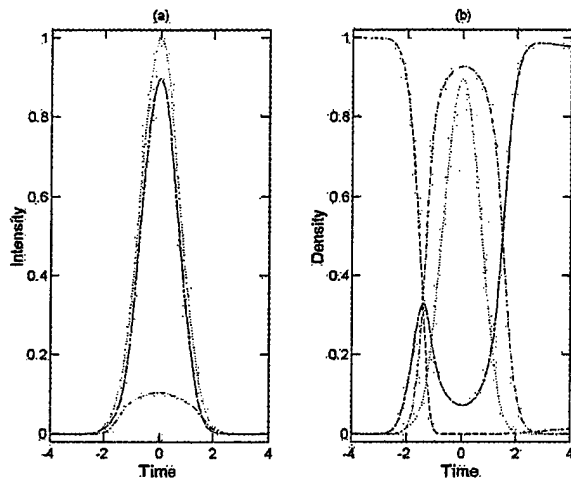


(I)

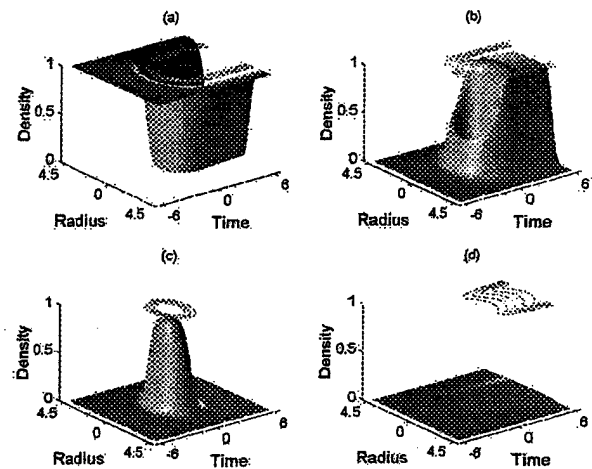


(II)

Fig. 8. Intensity and carrier density plots for input energy = 50 μ J: (I.a) the dotted line shows the normalized input pulse, the solid line shows the output pulse whose peak value = 0.40; (I.b) the dashed line shows the carrier density of state S_0 , whose minimum value is 0.13, the solid line shows the carrier density of state S_1 whose maximum value is 0.86, the dot-dashed line shows the carrier density of S_2 whose maximum value is 0.19; (II) shows the 3-D plots of the carrier densities at (a) the ground state, (b) the first excited singlet state, (c) the second excited singlet state, (d) the first excited triplet state.



(I)



(II)

Fig. 9. Intensity and carrier density plots for input energy = 1000 μJ : (I.a) the dotted line shows the normalized input pulse, the solid line shows the output pulse whose peak value = 0.72; (I.b) the dashed line shows the carrier density of state S_0 whose minimum value is 0.0, the solid line shows the carrier density of state S_1 whose maximum value is 0.99, the dot-dashed line shows the carrier density of S_2 whose maximum value is 0.99; (II) shows the 3-D plots of the carrier densities at (a) the ground state, (b) the first excited singlet state, (c) the second excited singlet state, (d) the first excited triplet state.

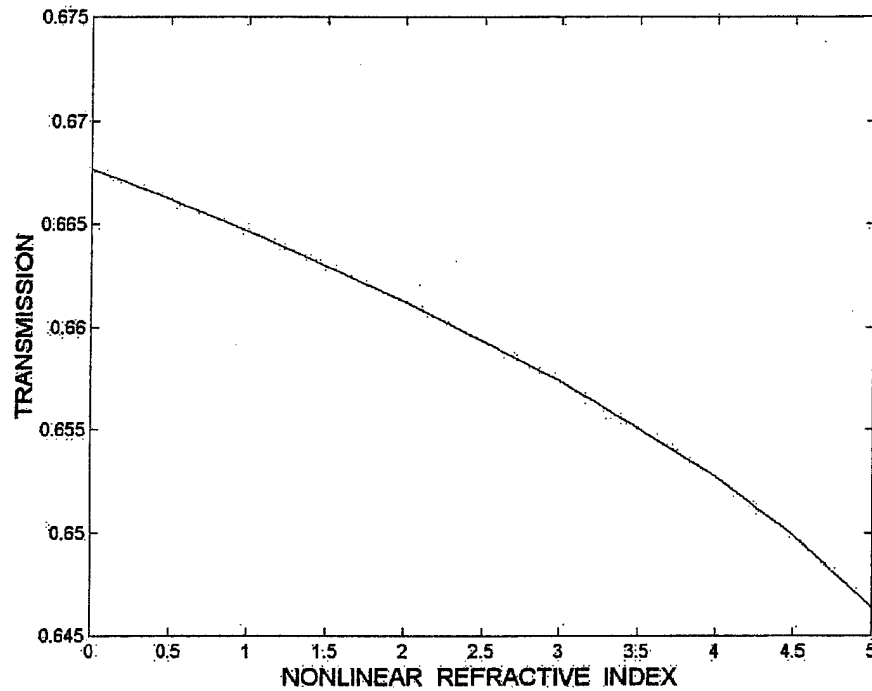


Fig. 10. Transmission as a function of the coefficient of the nonlinear index of refraction (n_2) in units of $10^{-17} \text{ cm}^2/\mu\text{W}$. The incident energy is $1 \mu\text{J}$ and the carrier density is $N_T = 6.022 \times 10^{16} \text{ cm}^{-3}$. The increased absorption is due to the self-focusing of the light arising from the nonlinear Kerr-effect.



(a)



(b)

Figure 11. (a) Kerr self-focusing (b) tandem optical limiter using self-focusing before nonlinear absorber.

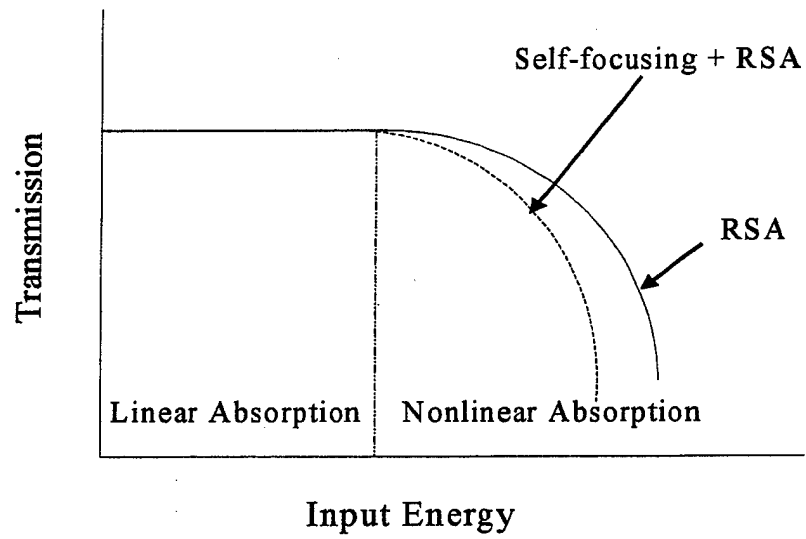


Figure 12. Schematic diagram of transmission of tandem optical limiter using self-focusing.

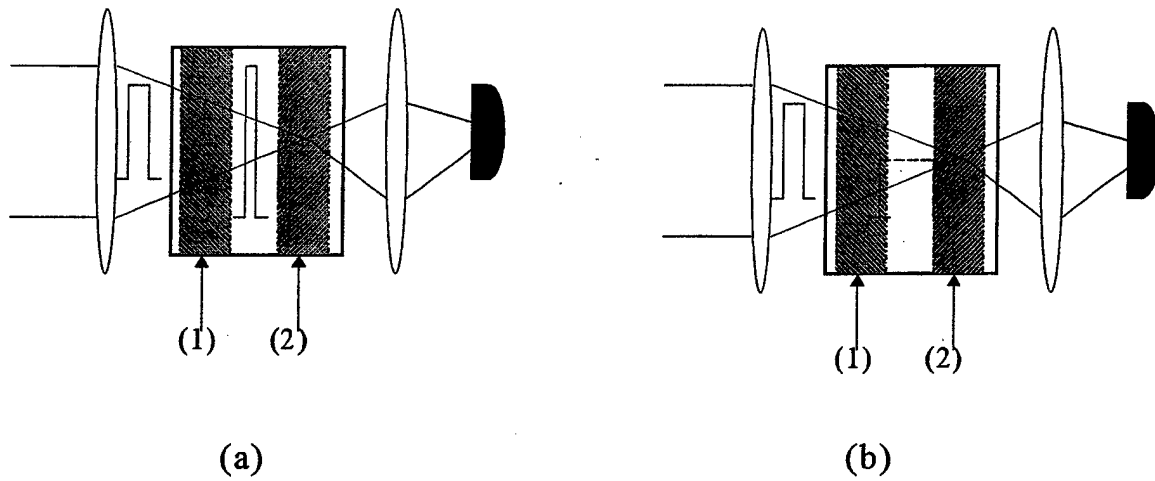
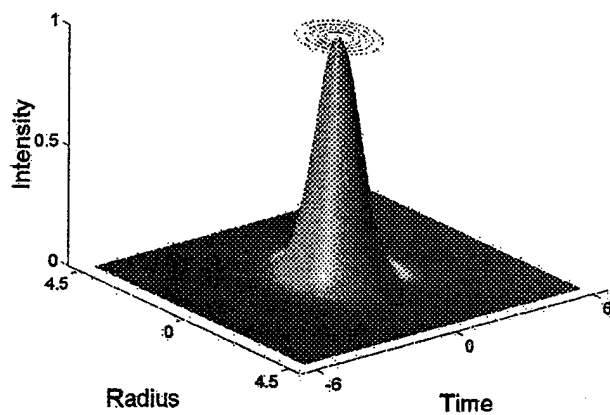
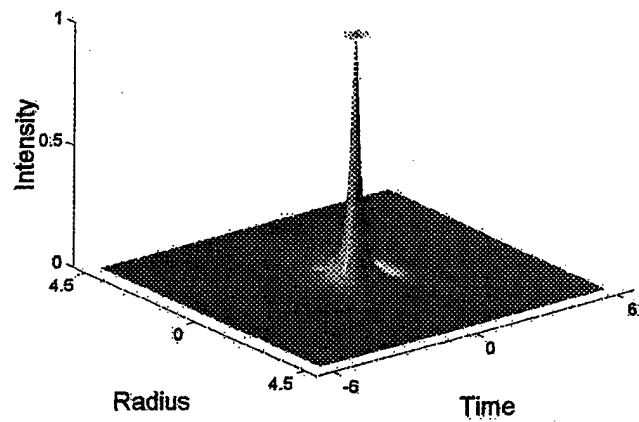


Figure 13. Pulse reshaping in a tandem optical limiter using Kerr nonlinearity and GVD in element (1) and nonlinear absorption in element (2); (a) pulse compression, (b) pulse broadening.



(a)



(b)

Fig 14. (a) Gaussian input pulse with its peak value normalized to 1. (b) The pulse shape after propagating one diffraction length in a nonlinear dispersive material ($NL=2.0$, $GVD=-0.05$); its peak value is 18 even though in the graph z axis value is normalized to 1.

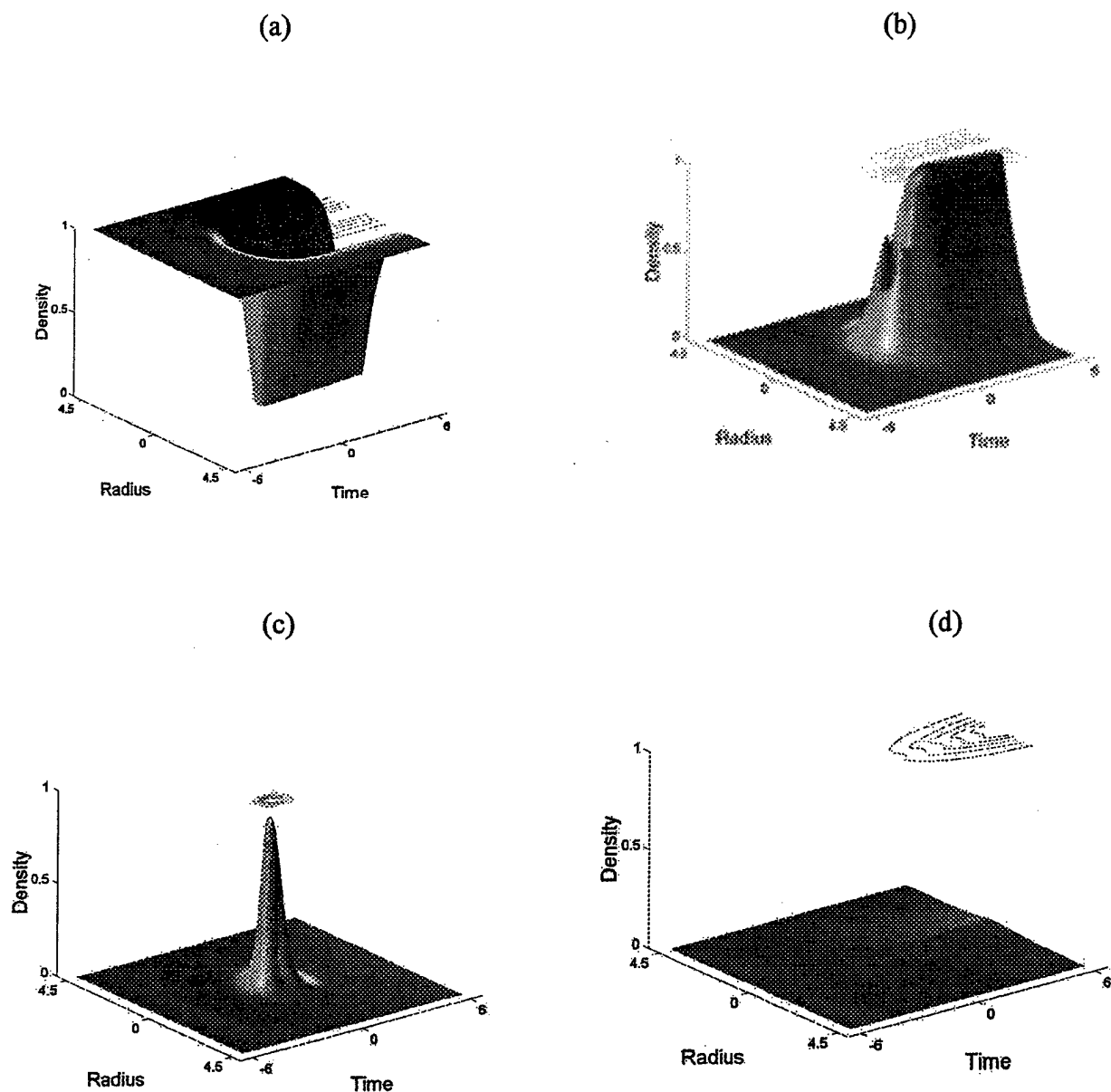


Fig. 15. Carrier density population profiles at a propagation distance of one diffraction length in the nonlinear material and 0.7 mm in the RSA material. The input energy is 50 uJ. (a) The ground level, min. value= 2.3×10^{-5} . (b) The first excited singlet (S1) state, max. value= 0.984 (c) The second excited singlet (S2) state, max value=0.912. (d) The first excited triplet (T1) state, max value= 0.019.

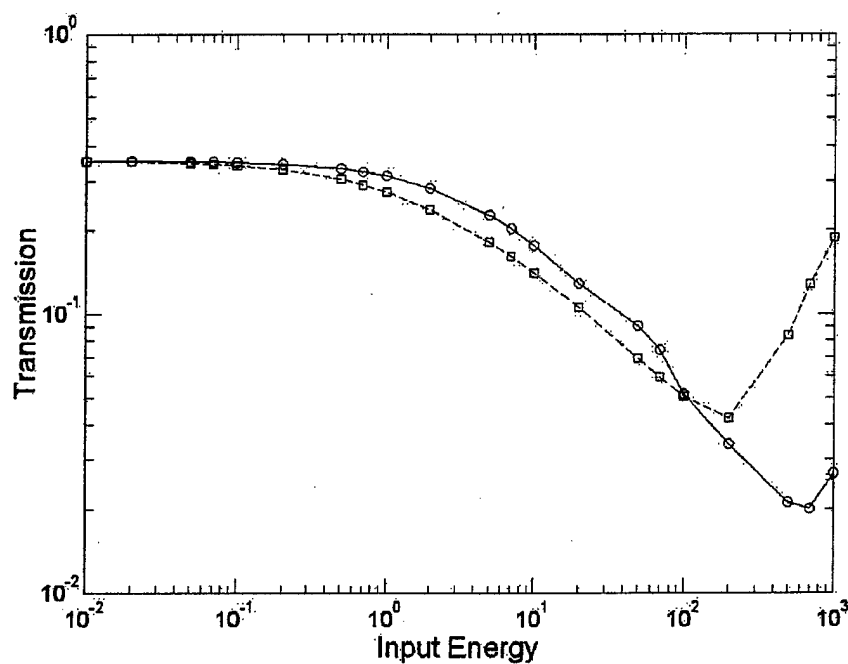
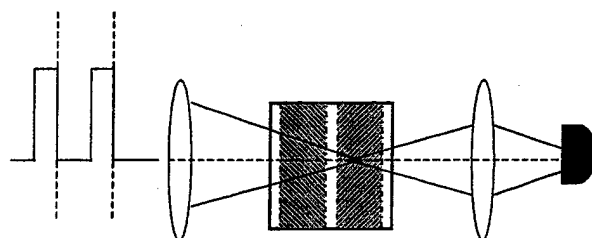
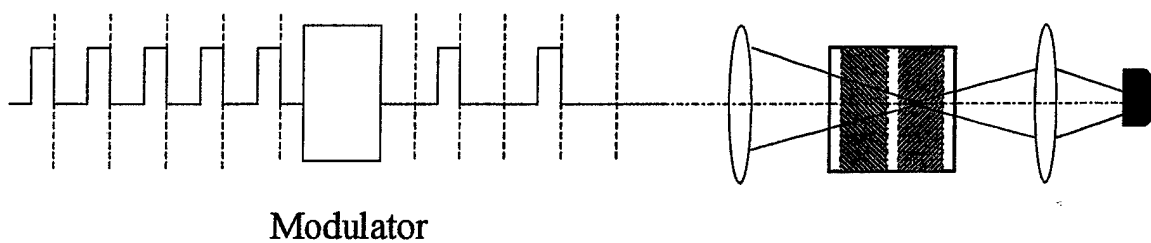


Fig. 16. Input energy vs. transmission for of one-diffraction length (NL +GVD) and 0.72 mm propagation through RSA. The circle data points are for NL=0.0, GVD=0.0 case. The square data points are for NL=2.0, GVD=-0.05 case.



(a)



(b)

Fig. 17. Schematic diagrams of possible optical beam processing for numerical calculation of optical limiting: (a) multiple input pulses; (b) randomization of temporal pulses using a modulator.

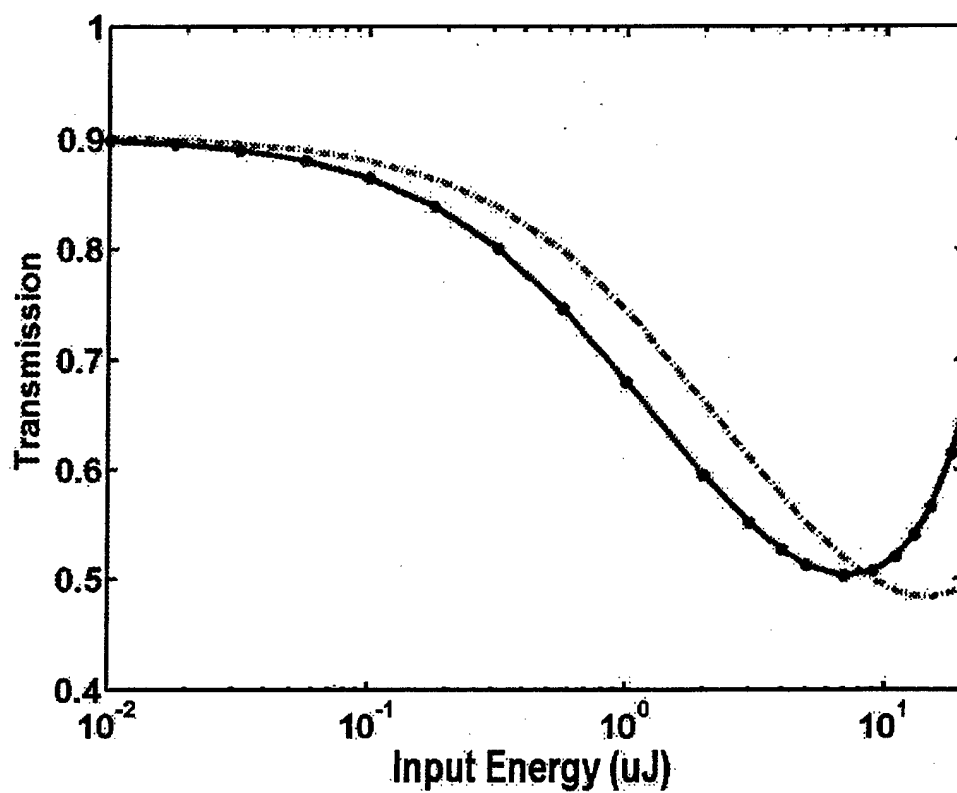


Fig. 18. Transmission versus input energy for $\tau_r=2$ and 10.

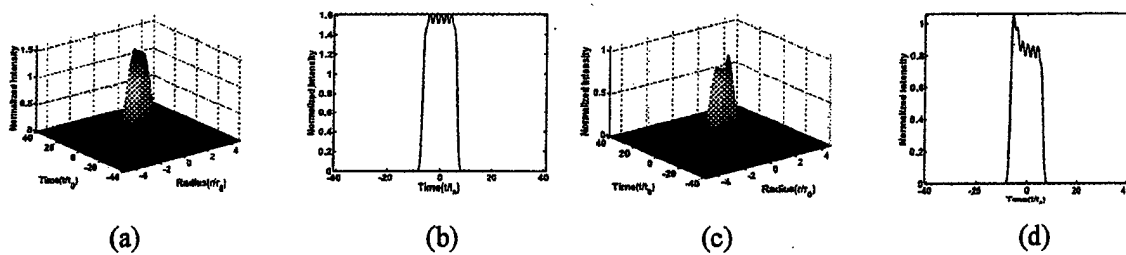


Fig. 19. Normalized intensity curves for input energy = $9\mu\text{J}$ and $\tau_r=2$; (a) and (b) before excited-state absorber; (c) and (d) after excited-state absorber.

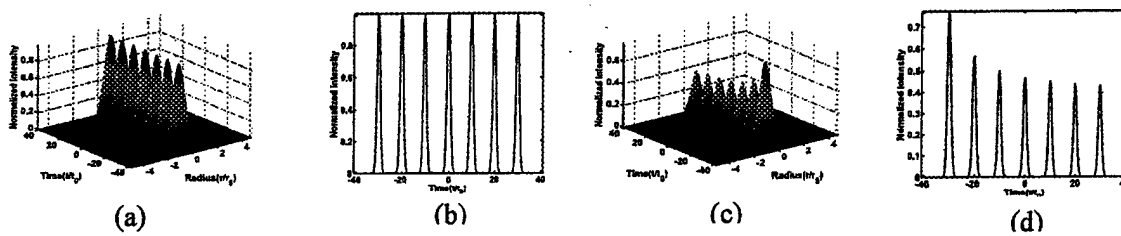


Fig. 20. Normalized intensity curves for input energy = $9\mu\text{ J}$ and $\tau_r=10$; (a) and (b) before excited-state absorber; (c) and (d) after excited-state absorber.